Resonance and Structural Assignment in (Car)Borane Clusters Using ^{11}B Residual Quadrupolar Couplings

Franziska Rüttger, Dietmar Stalke and Michael John

Electronic Supporting Information

Table of Contents

Experimental procedures

General procedures

Compounds **1** (*ortho*-carborane), **2** (*meta*-carborane) and **4** (decaborane) were obtained from abcr chemicals and used without further purification. The air sensitive compound **4** was stored and handled in an argon dry box. NMR measurements were performed on a Bruker Avance III HD 400 MHz spectrometer equipped with a BBFO smart probe and a z-gradient coil, a Bruker Avance III HD 500 MHz spectrometer equipped with a BBO cryoprobe prodigy and a z-gradient coil and a Bruker Avance NEO 600 MHz spectrometer equipped with TBI and TBO probes with z-gradient coils. All spectra were measured at 298 K if not stated otherwise. For alignment tensor determination and graphical representation, the software MSpin[1] was used. DFT calculations were performed using Gaussian16[2] at the B3LYP/Def2TZVP[3] level of theory in the gas phase. The graphic representation of the EFG tensors were created using a notebook provided by J. Autschbach with Mathematica 13.1 (Wolfram Research Inc. Chamgaign, Illinois, USA).[4] NMR data processing was performed with TopSpin 4.0.8 and data analysis was performed with TopSpin 4.0.8 and MestReNova 14.1.2.

Preparation of polystyrene sticks

Styrene was separated from its radical inhibitor using a dry column packed with silica gel and dried over magnesium sulfate. The purified styrene was transferred into a Schlenk flask and degassed using three freeze-pump cycles. Then, 0.4 Vol% of 1,3-divinylbenzene (DVB) was added while stirring. The mixture was transferred into glass tubes with 3.8 mm inner diameter in a Schlenk flask under inert gas atmosphere and was polymerized at 115°C for three days. Afterwards, the glass tubes were broken and the homogeneous parts of the polymer were cut into sticks of about 1 – 1.5 cm length. The polymer sticks were stored and handled in an argon dry box for the air sensitive compound **4** and in a flask without exclusion of air for air stable compounds (**1**-**3**).

NMR sample preparation

Isotropic air stable samples (**1**-**3**) were prepared using Quartz NMR tubes with 5 mm outer and 4.2 mm inner diameter. The isotropic air-sensitive sample of **4** was prepared in an argon dry box using standard Young tubes with 5 mm outer and 4.2 mm inner diameter. For the preparation of anisotropic samples of **1**-**3**, the compound of interest (ca. 20 mg) was dissolved in 0.5 mL THF-d_8 and the solution was transferred into a 5 mm Quartz NMR tube. For **4**, this procedure was carried out in an argon dry box. A polystyrene stick was inserted into the NMR tube held horizontally until it was positioned in the active region of the NMR coil. The tube was sealed with a rubber cap, could be put back into an upright position after 5-10 minutes and was stored in the refrigerator at 3°C until measured.

Measurement of experimental RDCs and RQCs

For the measurement of experimental RDCs (D_{XH}, X = C, B), proton coupled ^{13}C spectra were recorded to obtain C-H splittings and $^{1}H,^{11}B$ HMQC were recorded to obtain B-H couplings in both isotropic and anisotropic samples, yielding the scalar coupling J_{XH} and the total coupling $T_{XH} = J_{XH} + D_{XH}$, respectively. Experimental RQCs were measured using the relevant $^{11}B\{^{1}H\}$ spectra in oriented phases. For the overlapped signal at -12.71 ppm in the anisotropic $^{11}B\{^{1}H\}$ spectrum of **3**, the RQC was obtained using lineshape fitting. Because the alignment in the polymer develops continuously during the swelling process, it is important that RDCs and RQCs are measured without large time delays between the experiments. Only then can both values be safely compared.

^{1}H,^{11}B-HMQC experiment with reduced ^{11}B flip angle

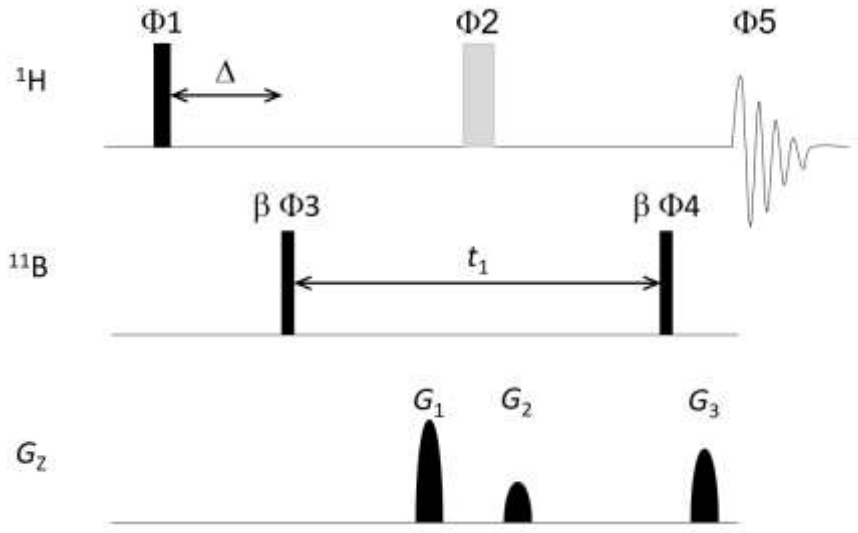

Figure S1. Pulse sequence (based on the hmbcgpndqf sequence) used for recording ^{1}H,^{11}B-HMQC spectra in this work. All spectra were acquired in magnitude mode with 1k x 128 data points with $\Delta = 1/(2 \cdot {}^{1}J_{BH}) = 3.3$ ms and ^{11}B flip angles of typically β = 30-45°. Phase cycle: $\Phi1 = x$, $\Phi2 = x_2(-x)_2$, $\Phi3 = x(-x)$, $\Phi4 = x_4(-x)_4$ and $\Phi5 = x(-x)x(-x)_2x(-x)x$. Gradient strengths: G_1 = 40%, G_2 = 30% and G_3 = 32.5%.

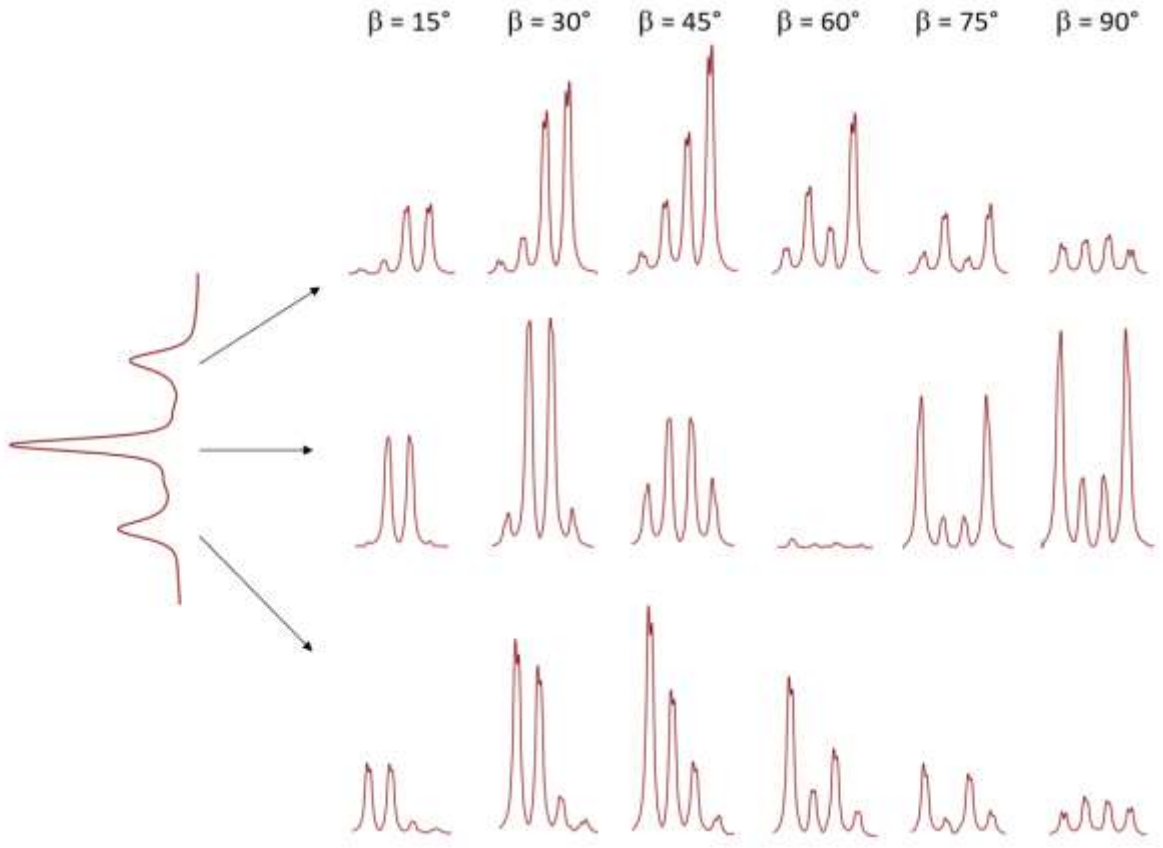

Figure S2. Horizontal (F2) slices of the ^{1}H,^{11}B HMQC experiment (^{1}H = 600.3 MHz) shown in **Figure S1** taken at each line of the ^{11}B quadrupolar triplet at −16.85 ppm of **2** as a function of the flip angle β. β = 30-45° turned out as good compromise between sensitivity and clean correlation of the ^{11}B transitions with the involved ^{11}B spin states indicating the sign of the ^{11}B RQC relative to ^{1}J(B-H).

NMR spectra

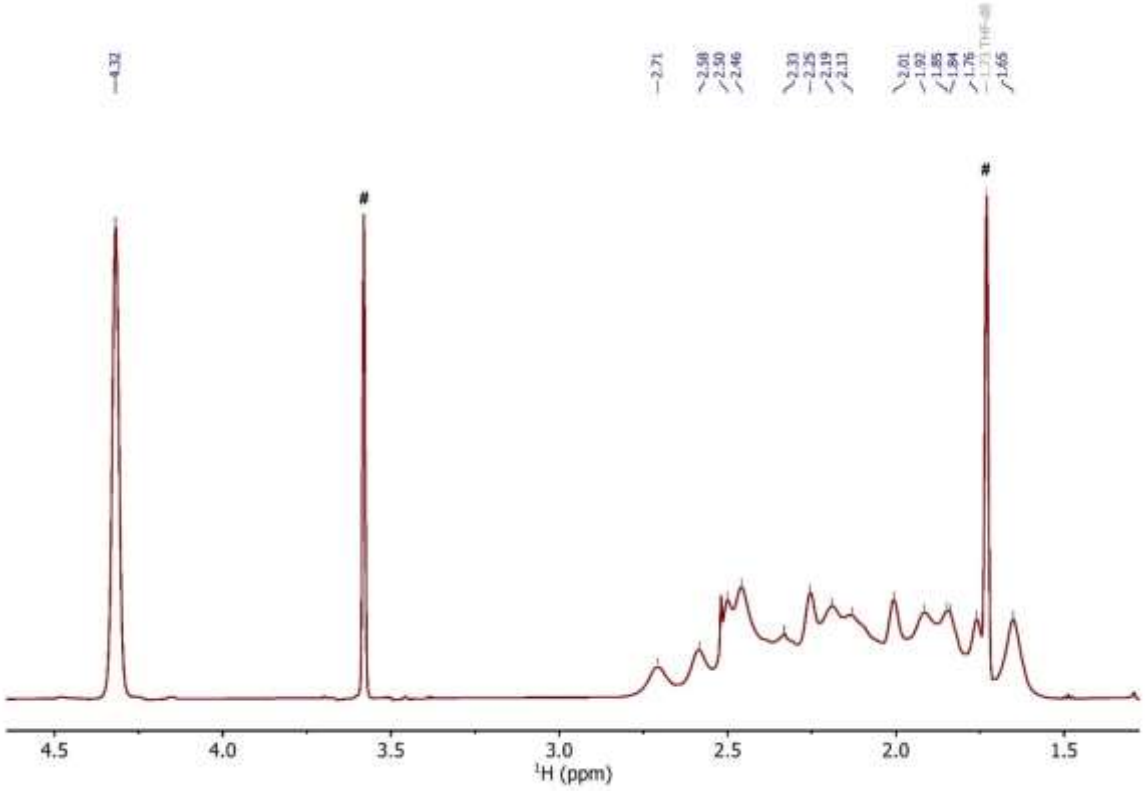

Figure S3. 600.3 MHz ^{1}H NMR spectrum of **1** in THF-d_8. Residual solvent signals are marked with #.

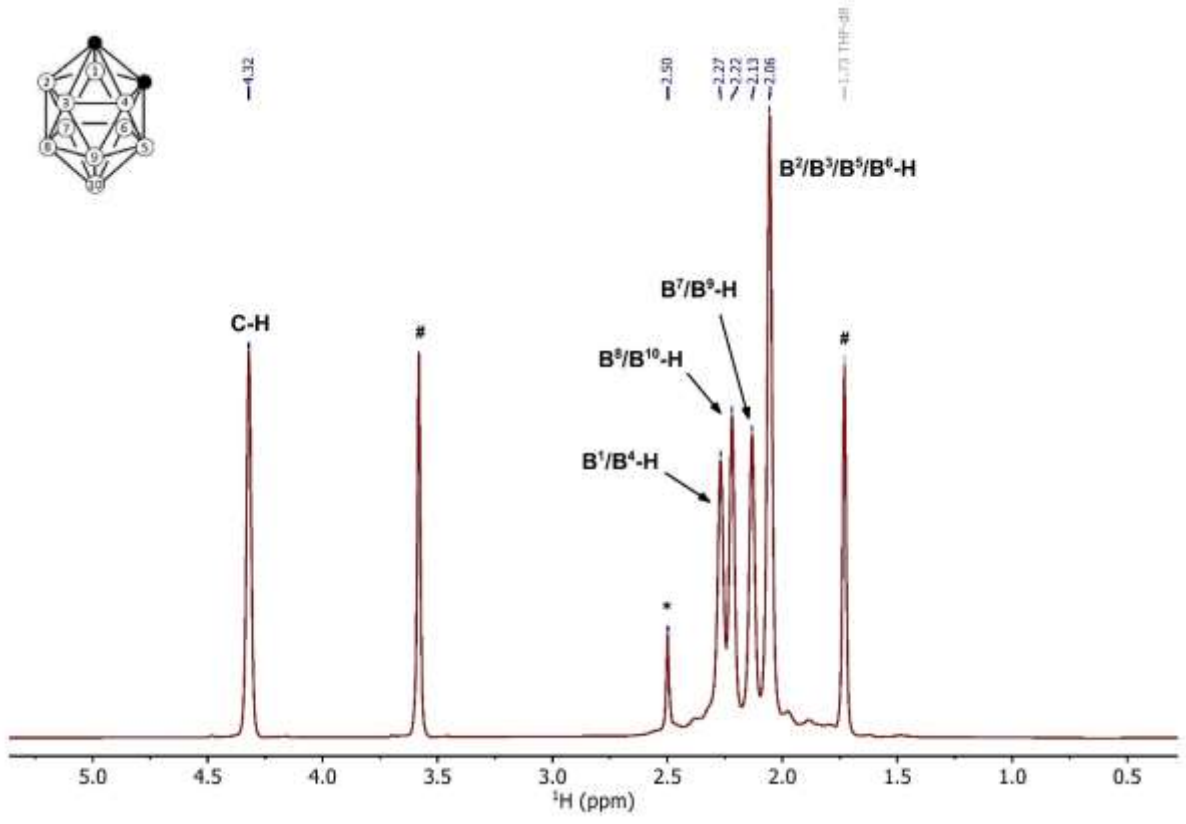

Figure S4. 600.3 MHz $^{1}H\{^{11}B\}$ NMR spectrum of **1** in THF-d_8. Residual solvent signals are marked with #. The signal marked with * is due to an impurity.

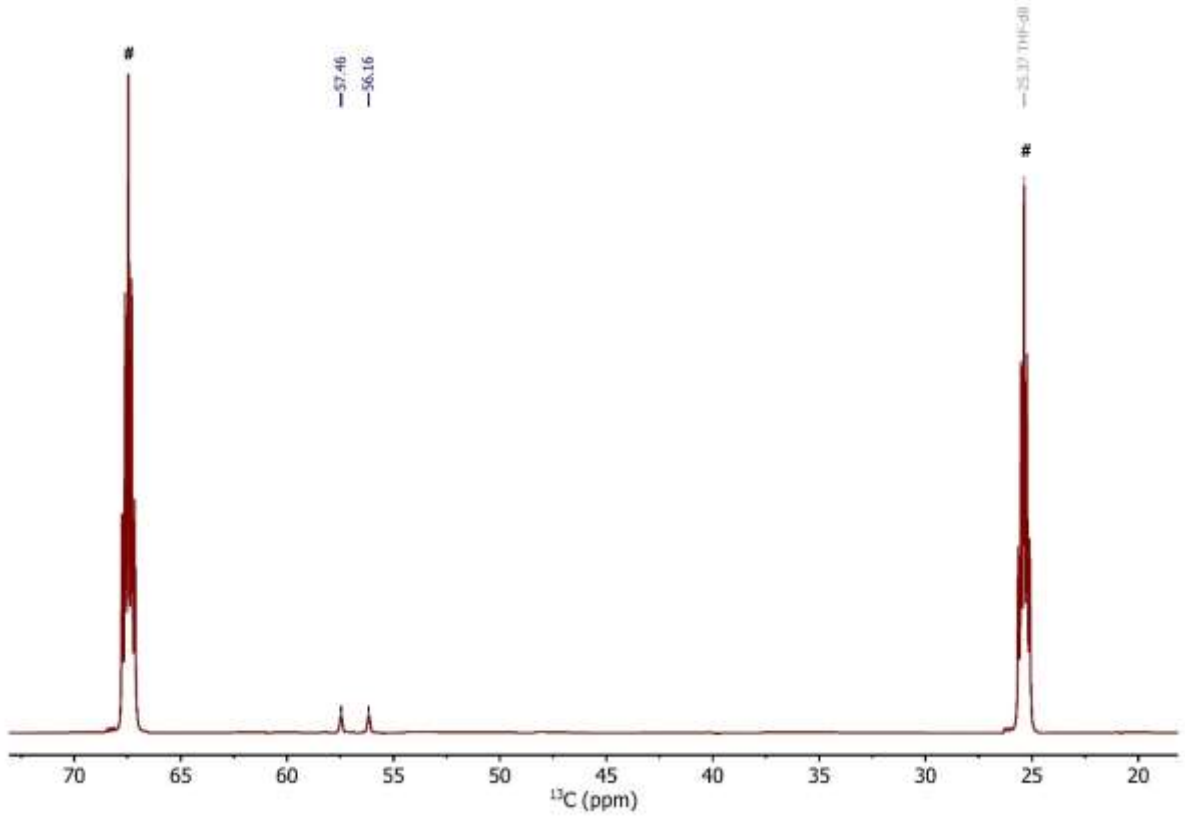

Figure S5. 150.9 MHz proton coupled ^{13}C NMR spectrum of **1** in THF-d_8. Solvent signals are marked with #.

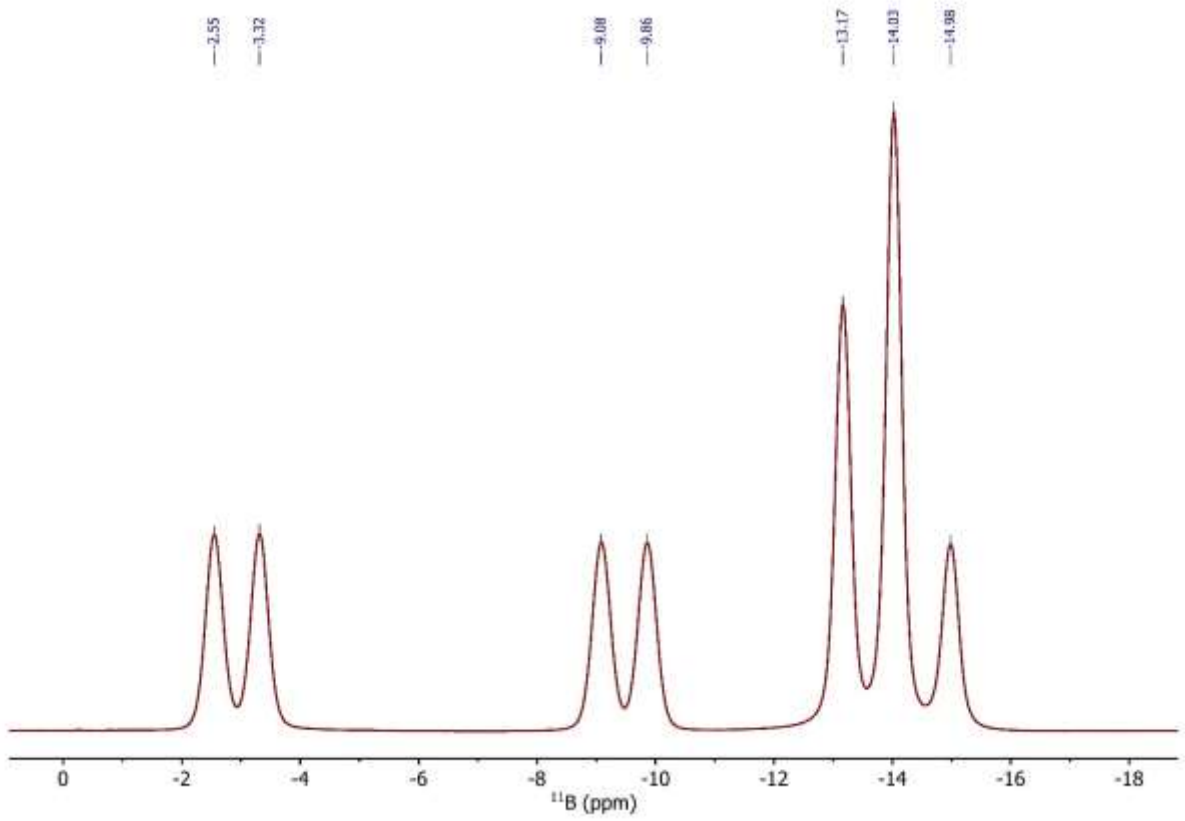

Figure S6. 192.6 MHz ^{11}B NMR spectrum of **1** in THF-d_8.

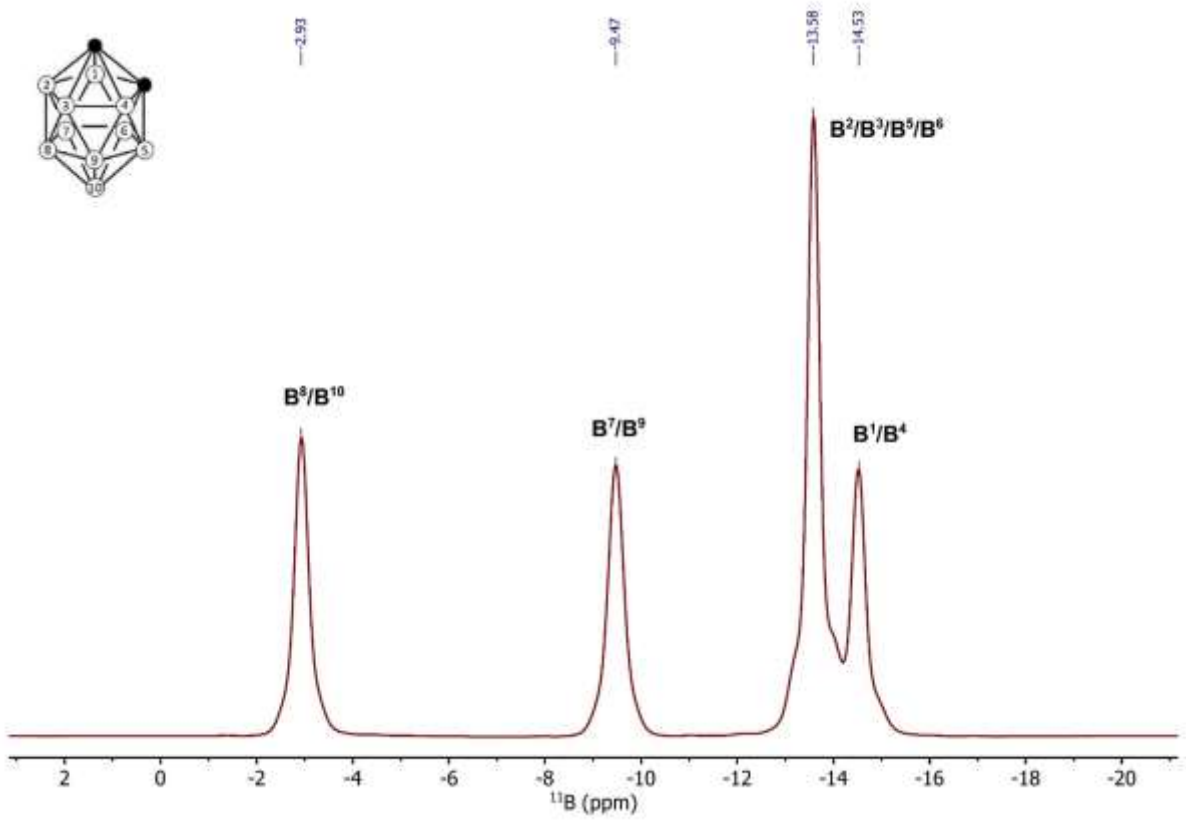

Figure S7. 192.6 MHz $^{11}B\{^{1}H\}$ NMR spectrum of **1** in THF-d_8.

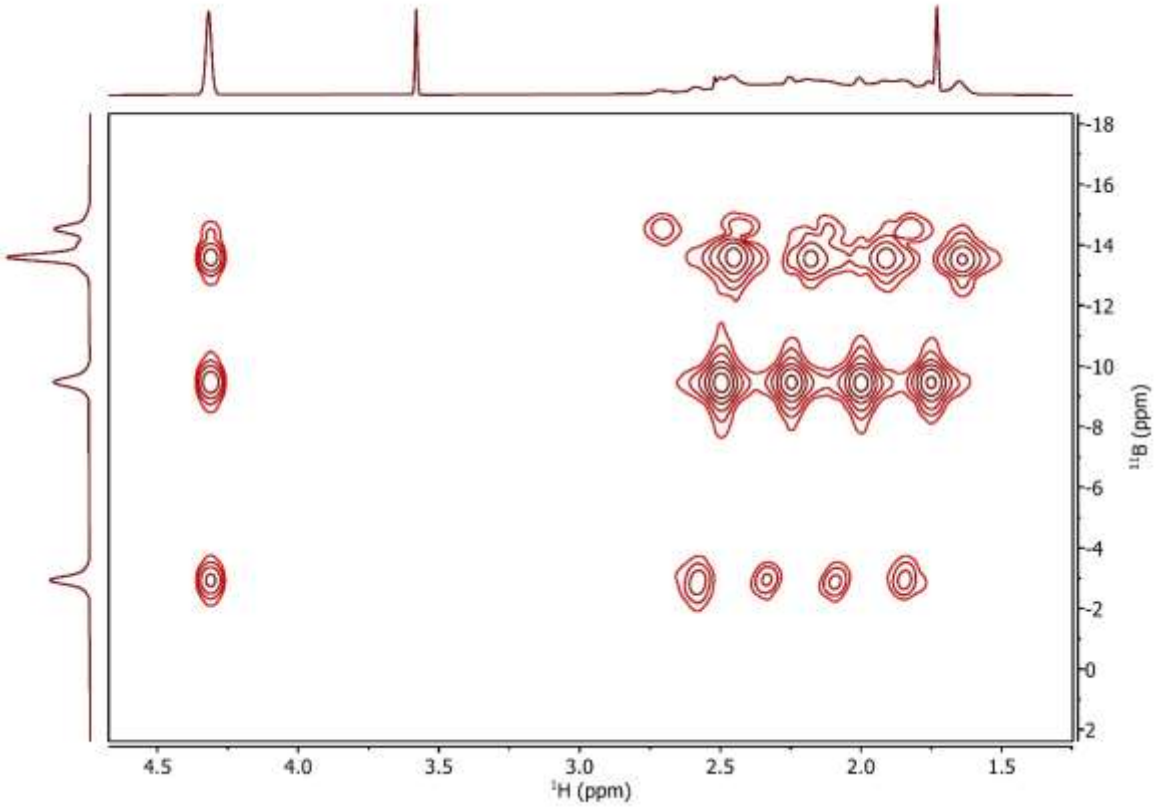

Figure S8. $^{1}H,^{11}B$ HMQC spectrum (^{1}H = 600.3 MHz) of **1** in THF-d_8.

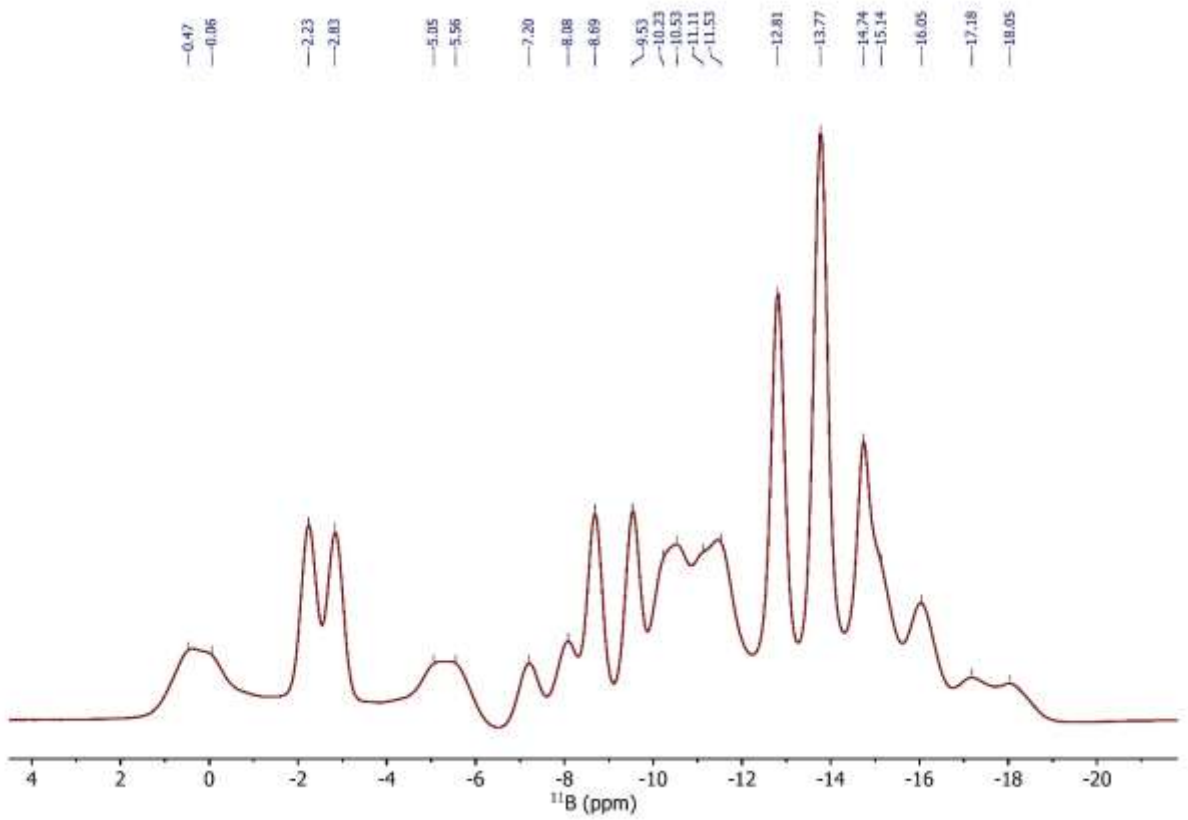

Figure S9. 192.6 MHz ^{11}B NMR spectrum of **1** in PS/THF-d_8 after 10 days of swelling.

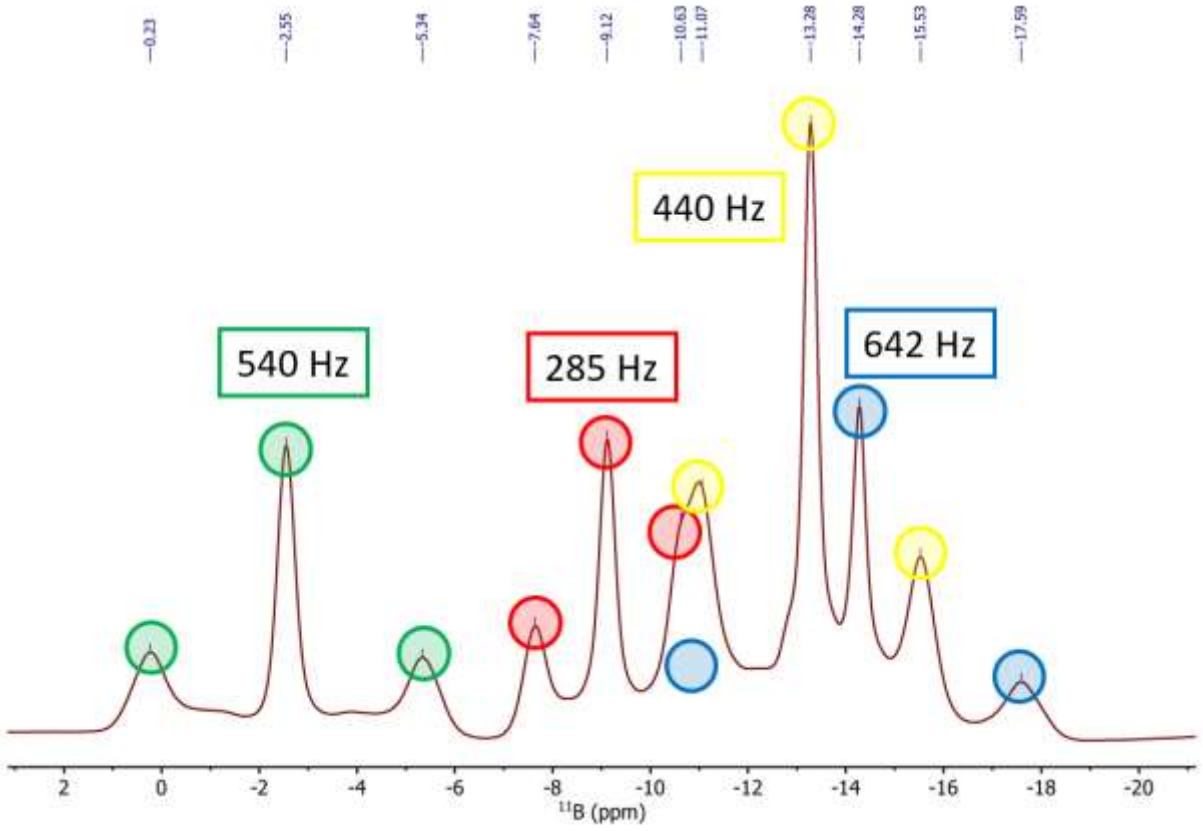

Figure S10. 192.6 MHz ^{11}B{^{1}H} NMR spectrum of **1** in PS/THF-d_8 after 10 days of swelling. The quadrupolar triplets are marked in different colours and labelled with absolute ^{11}B RQC values.

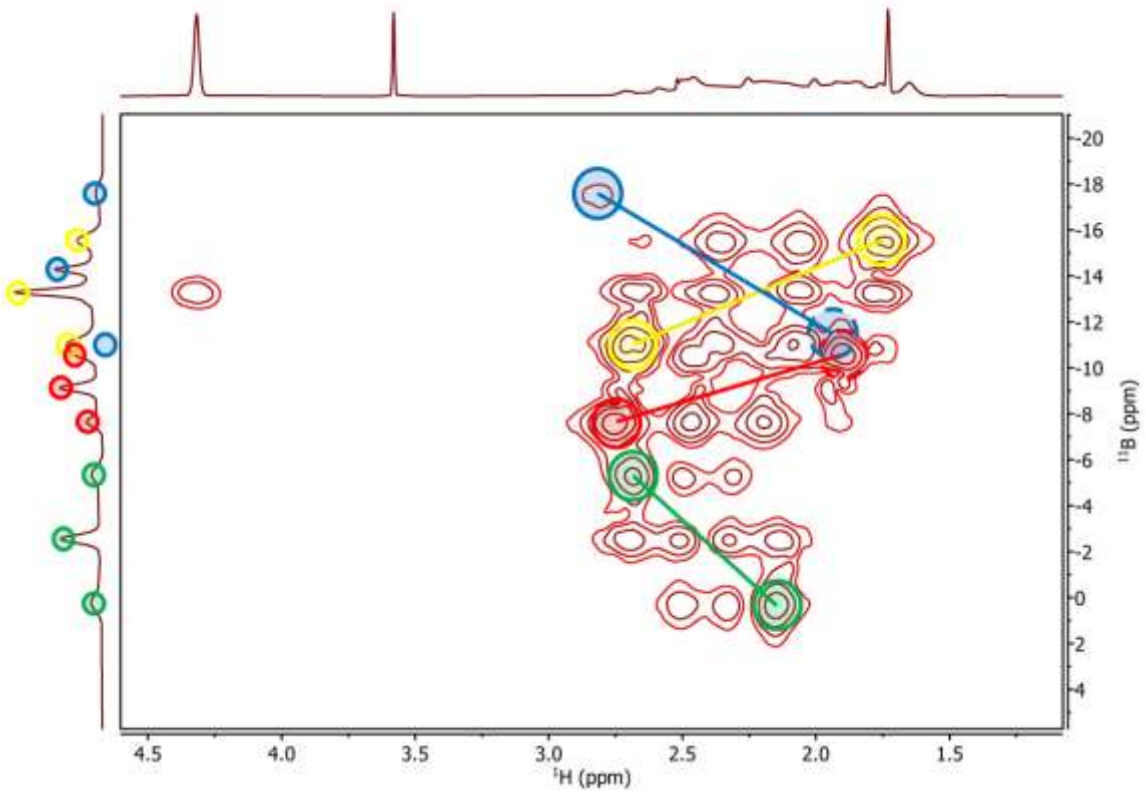

Figure S11. ^{1}H,^{11}B HMQC spectrum (^{1}H = 600.3 MHz, 45° ^{11}B flip angle) of **1** in PS/THF-d_8 after 10 days of swelling. The ^{1}H 1D trace is taken from the isotropic spectrum. The correlations that are crucial for the ^{11}B RQC sign determination are marked in the same colours as in **Figure S10**. The dashed circles mark overlapped satellite transitions.

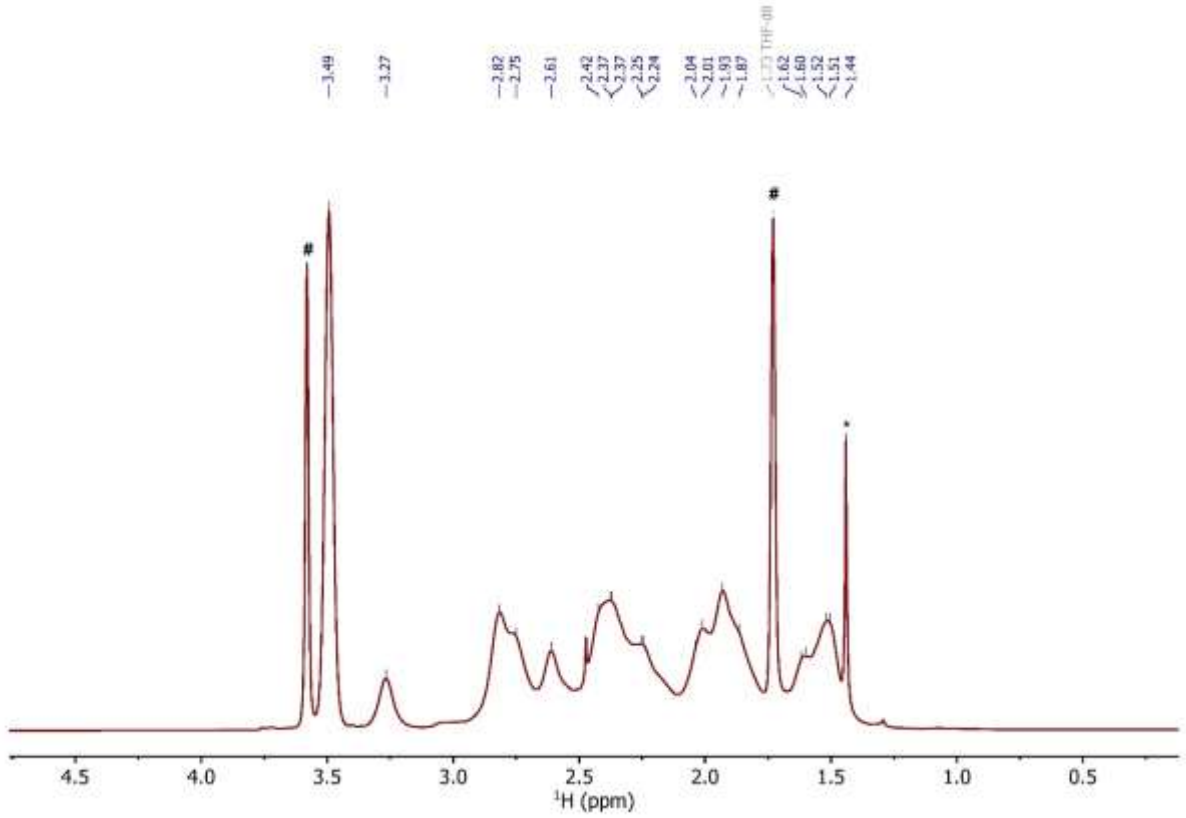

Figure S12. 400.3 MHz ^{1}H NMR spectrum of **2** in THF-d_8. Residual solvent signals are marked with #. The signal marked with * results from an impurity.

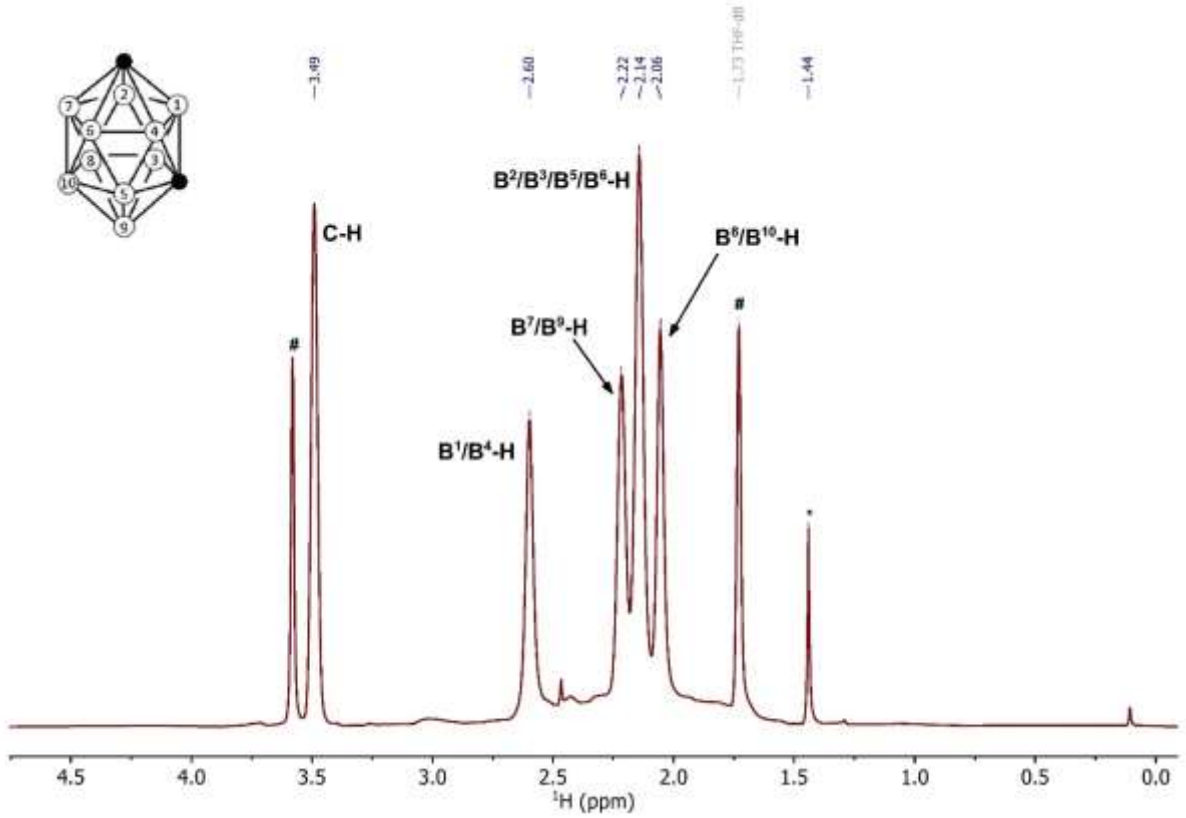

Figure S13. 400.3 MHz $^{1}H\{^{11}B\}$ NMR spectrum of **2** in THF-d_8. The residual solvent signals are marked with #. The signal marked with * is from an impurity.

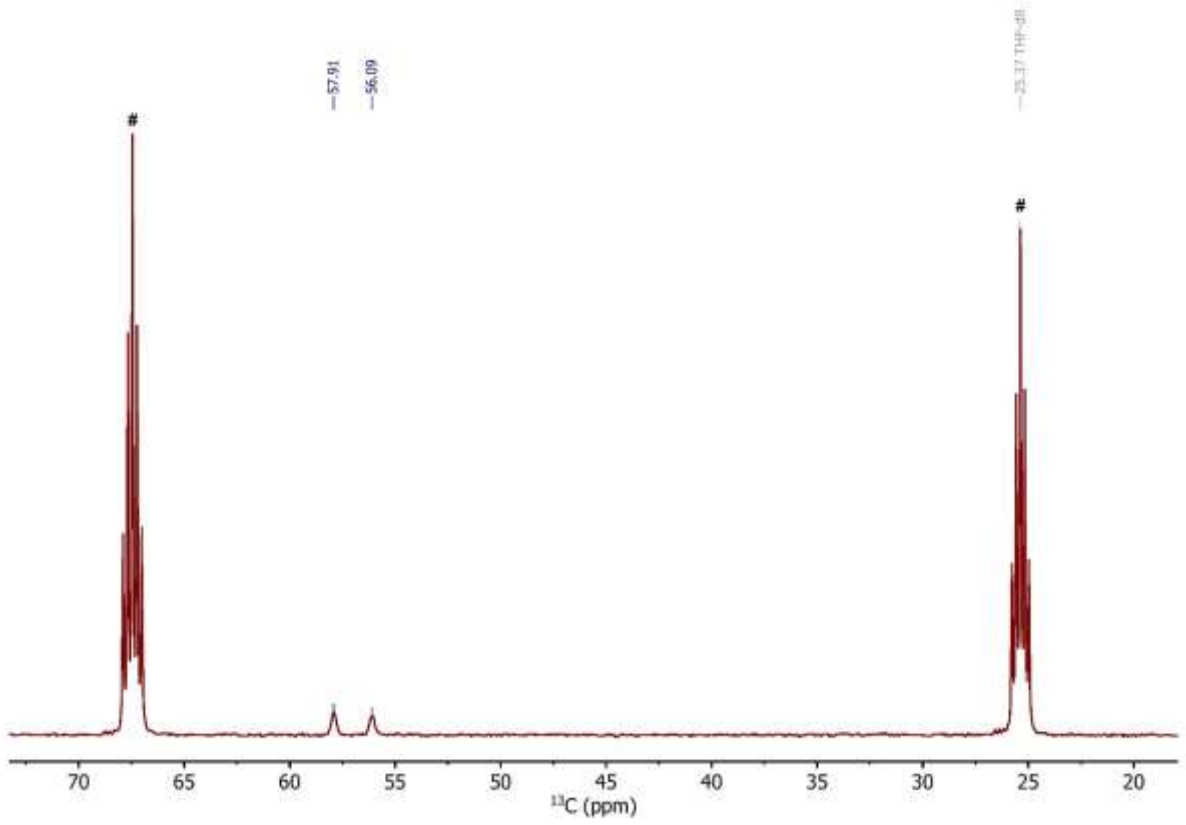

Figure S14. 100.6 MHz proton coupled ^{13}C NMR spectrum of **2** in THF-d_8. Solvent signals are marked with #.

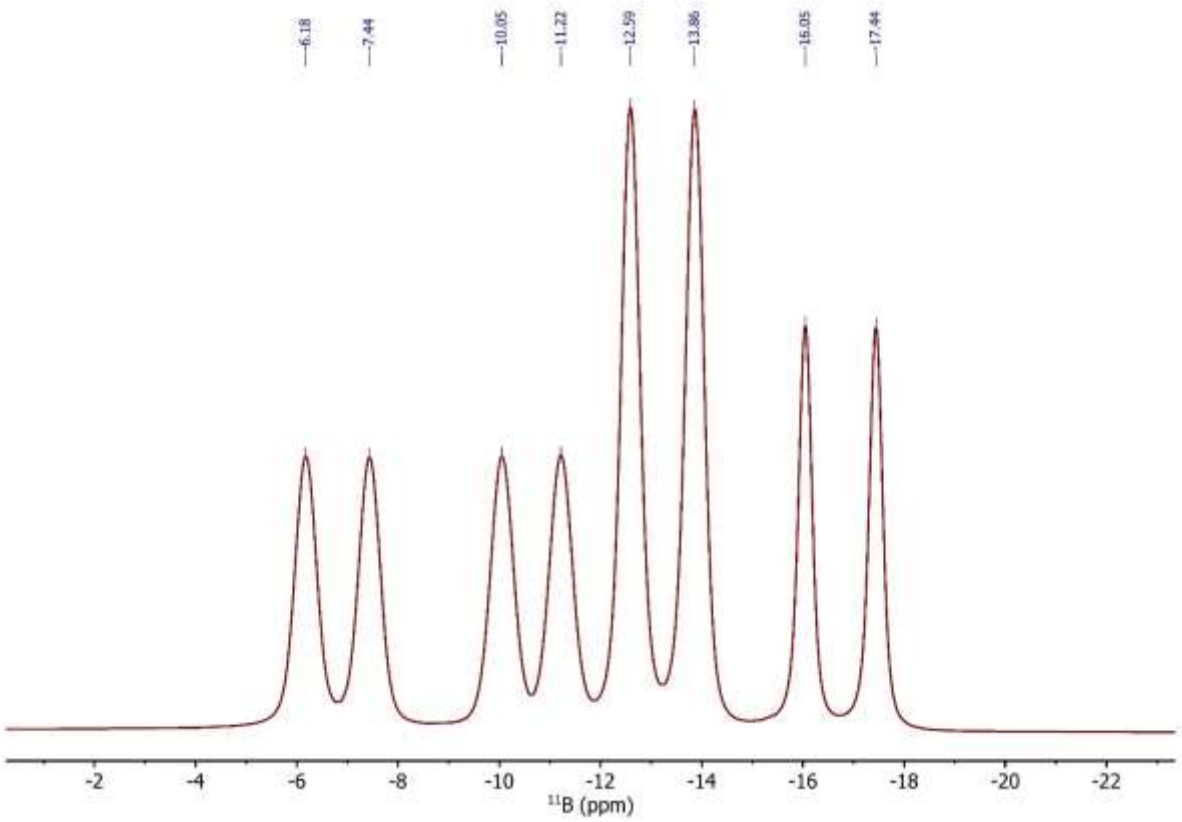

Figure S15. 128.4 MHz ^{11}B NMR spectrum of **2** in THF-d_8.

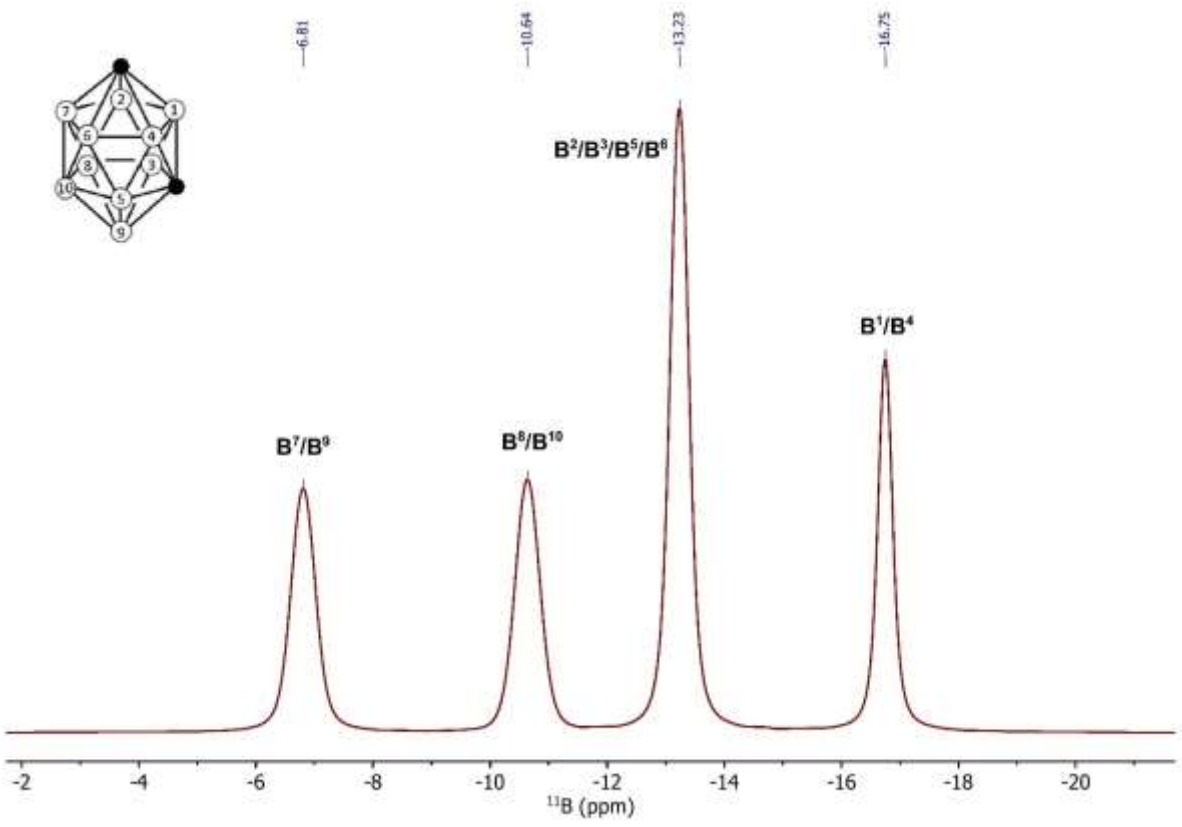

Figure S16. 128.4 MHz $^{11}B\{^1H\}$ NMR spectrum of **2** in THF-d_8.

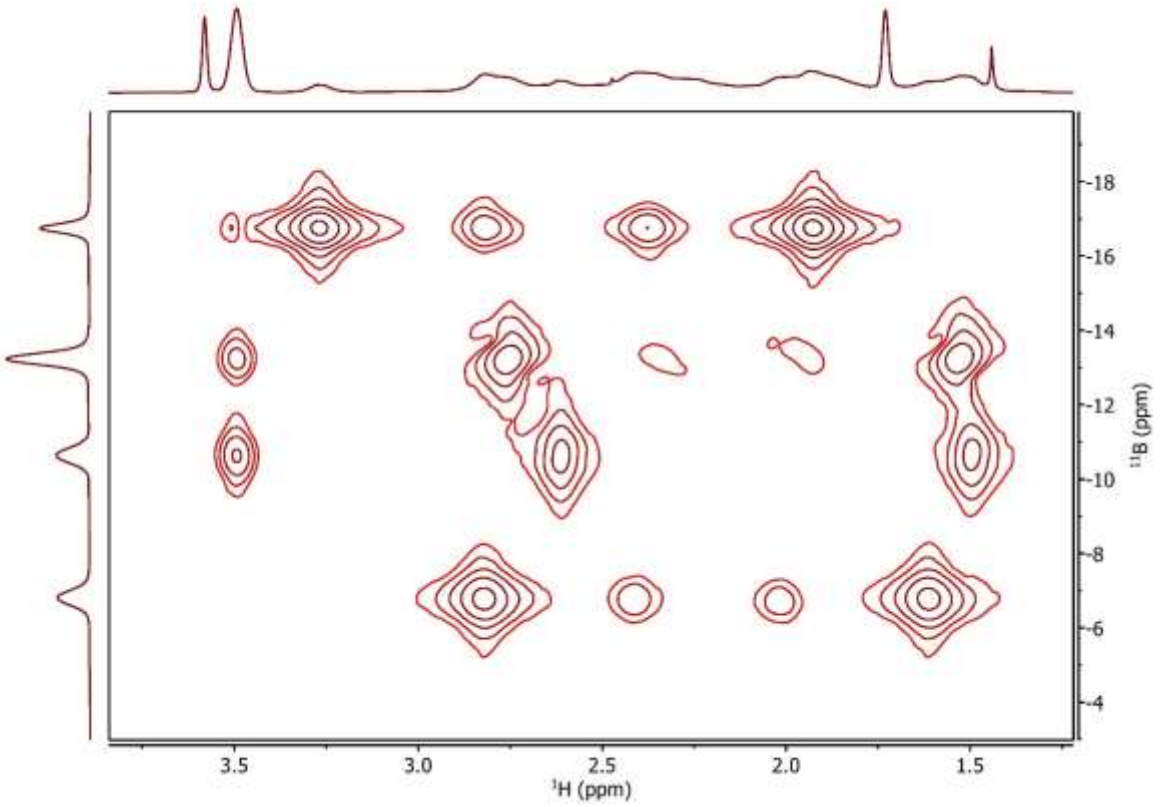

Figure S17. ^{1}H,^{11}B HMQC spectrum (^{1}H = 400.3 MHz) of **2** in THF-d_8.

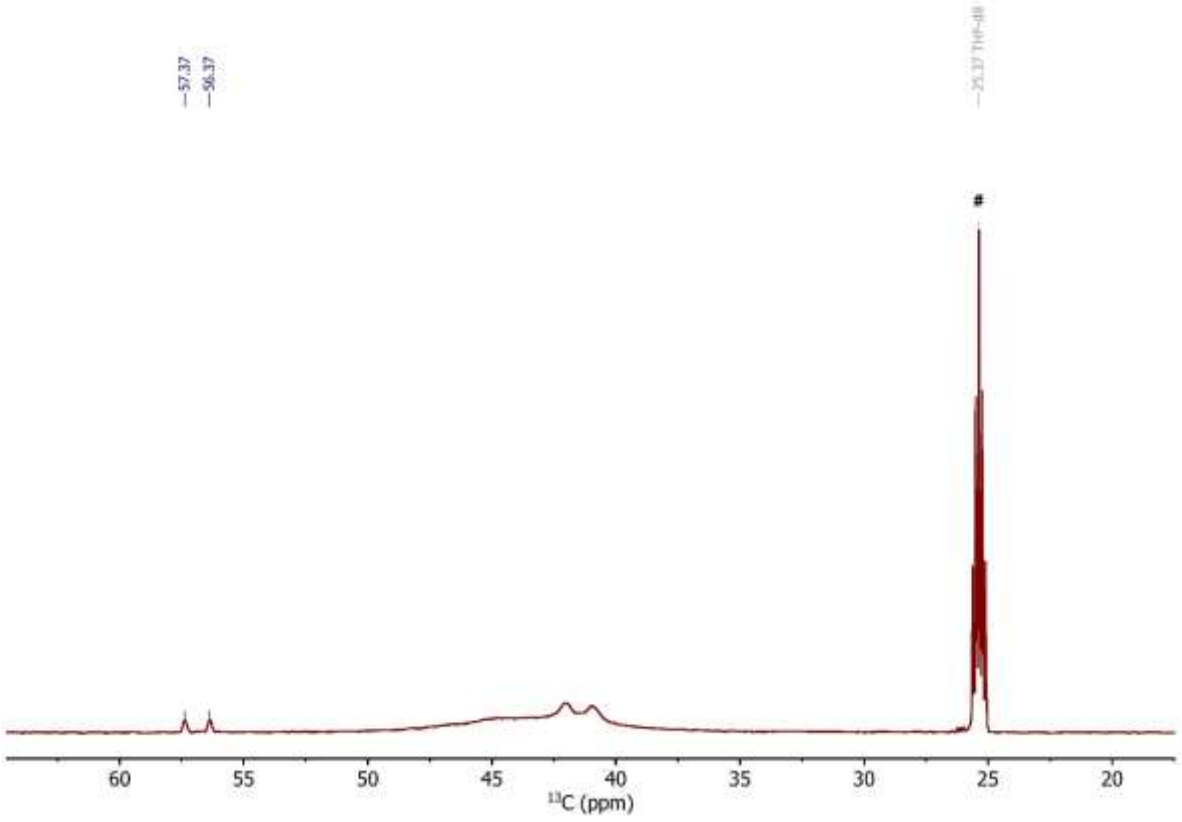

Figure S18. 150.9 MHz proton coupled ^{13}C NMR spectrum of in PS/THF-d_8 after 15 days of swelling. The solvent signal is marked with #. The broad signals between 40 and 50 ppm belong to the aliphatic carbons of polystyrene.

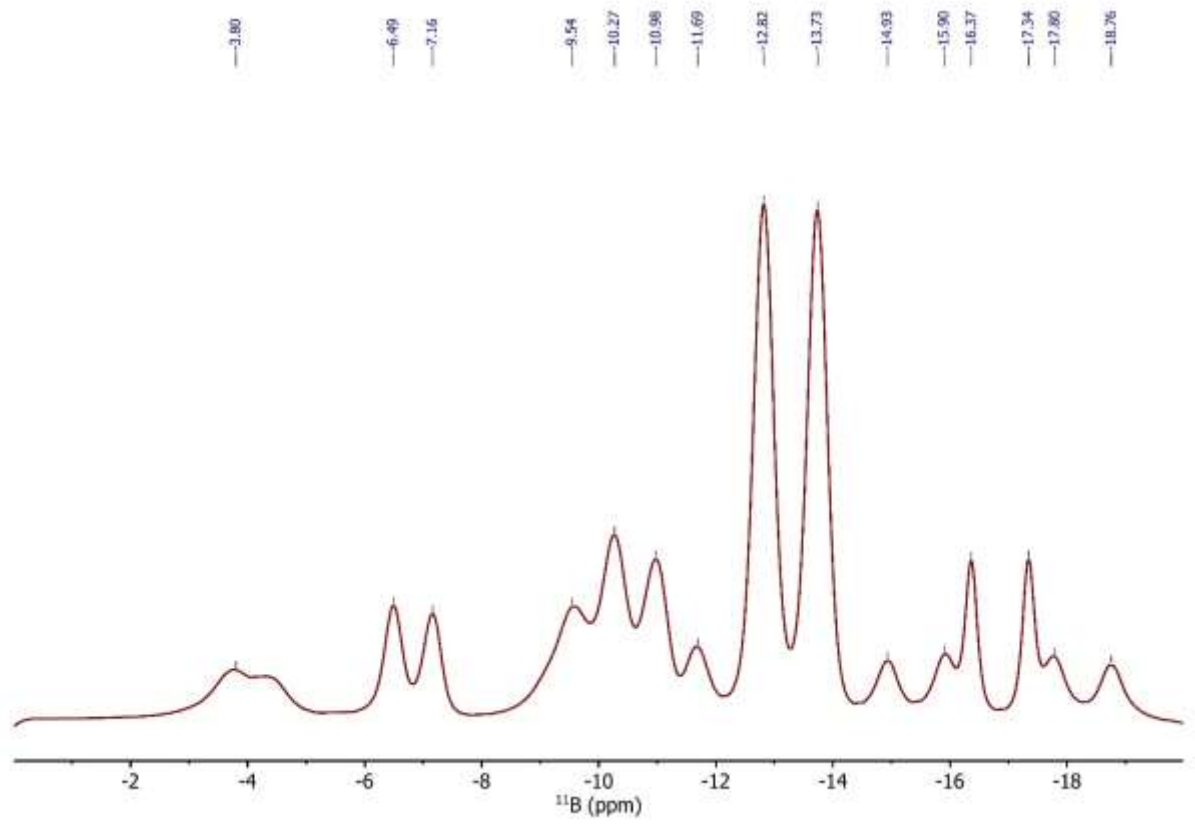

Figure S19. 192.6 MHz ^{11}B NMR spectrum of **2** in PS/THF-d_8 after 15 days of swelling.

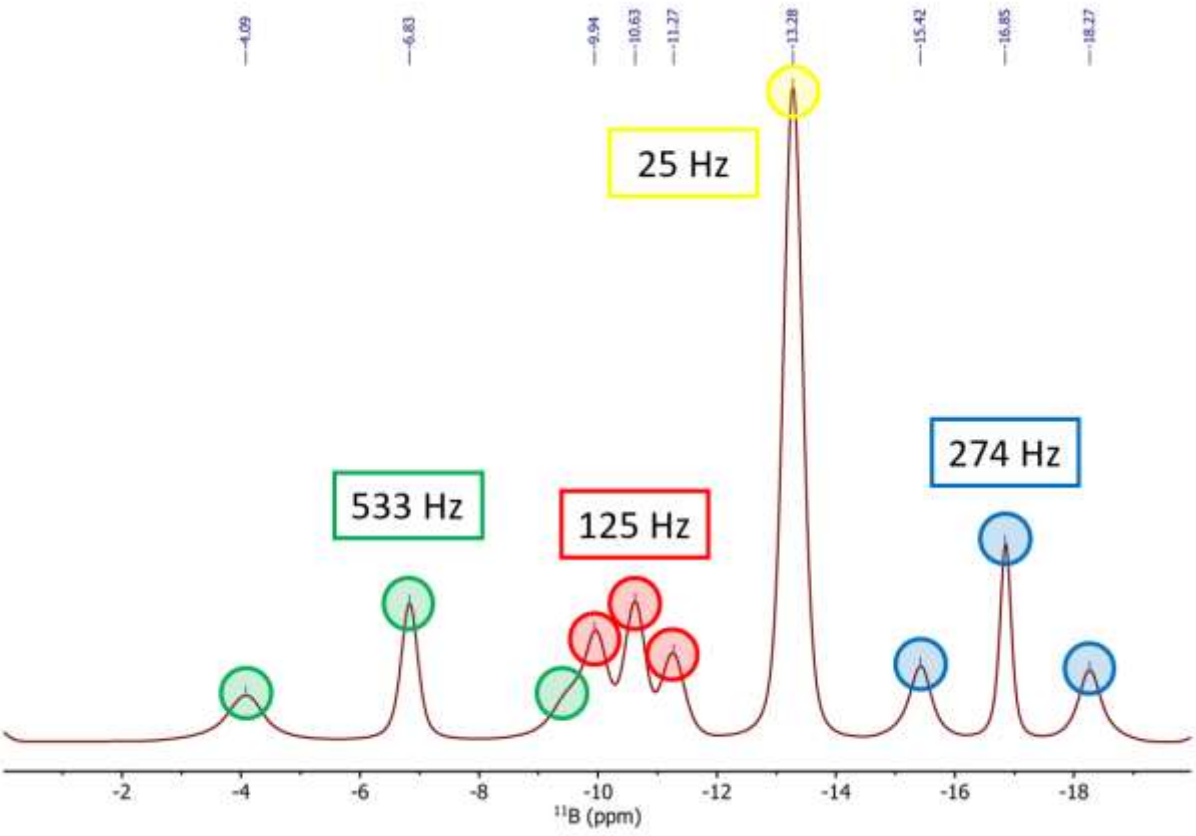

Figure S20. 192.6 MHz $^{11}B\{^1H\}$ NMR spectrum of **2** in PS/THF-d_8 after 15 days of swelling. The quadrupolar triplets are marked in different colours and labelled with absolute ^{11}B RQC values.

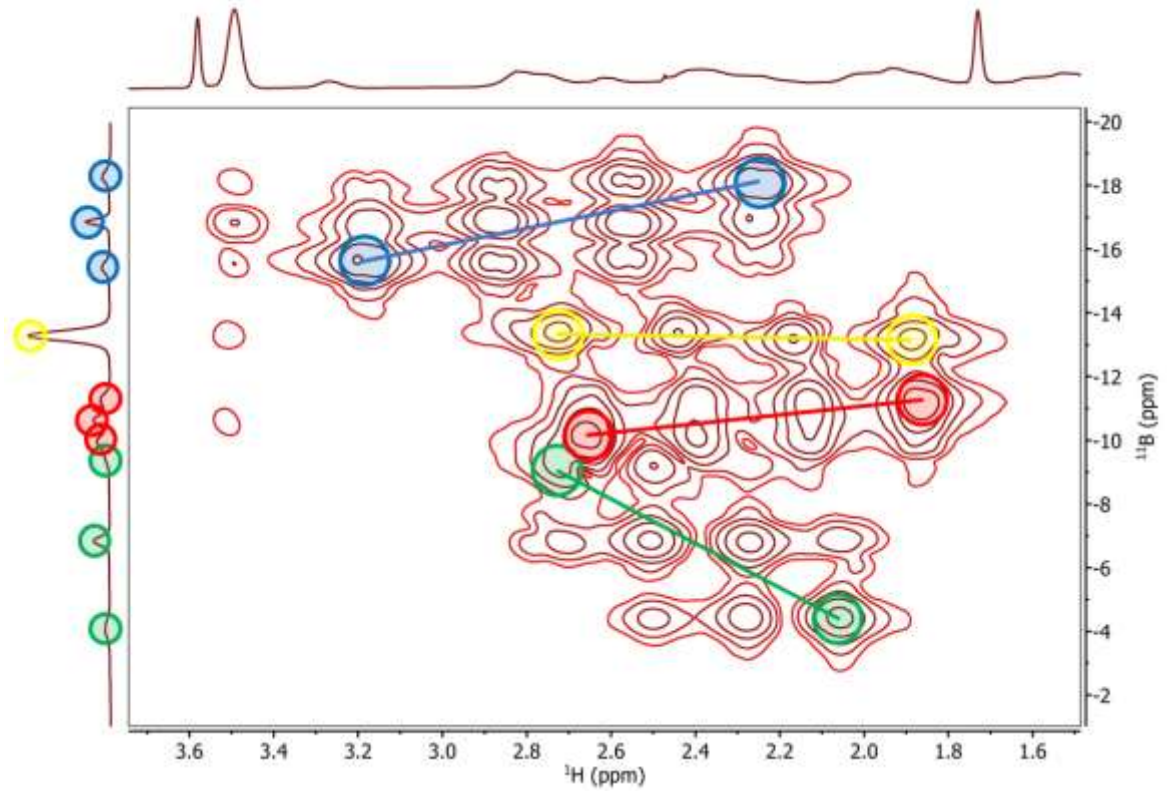

Figure S21. ^{1}H,^{11}B HMQC spectrum (^{1}H = 600.3 MHz, 45° ^{11}B flip angle) of **2** in PS/THF-d_8 after 15 days of swelling. The horizontal trace is taken from the isotropic ^{1}H 1D spectrum. The correlations that are crucial for the ^{11}B RQC sign determination are marked in the same colours as in **Figure S20**. The correlations marked in yellow show a slight negative tilt with a ^{11}B RQC of about −25 Hz.

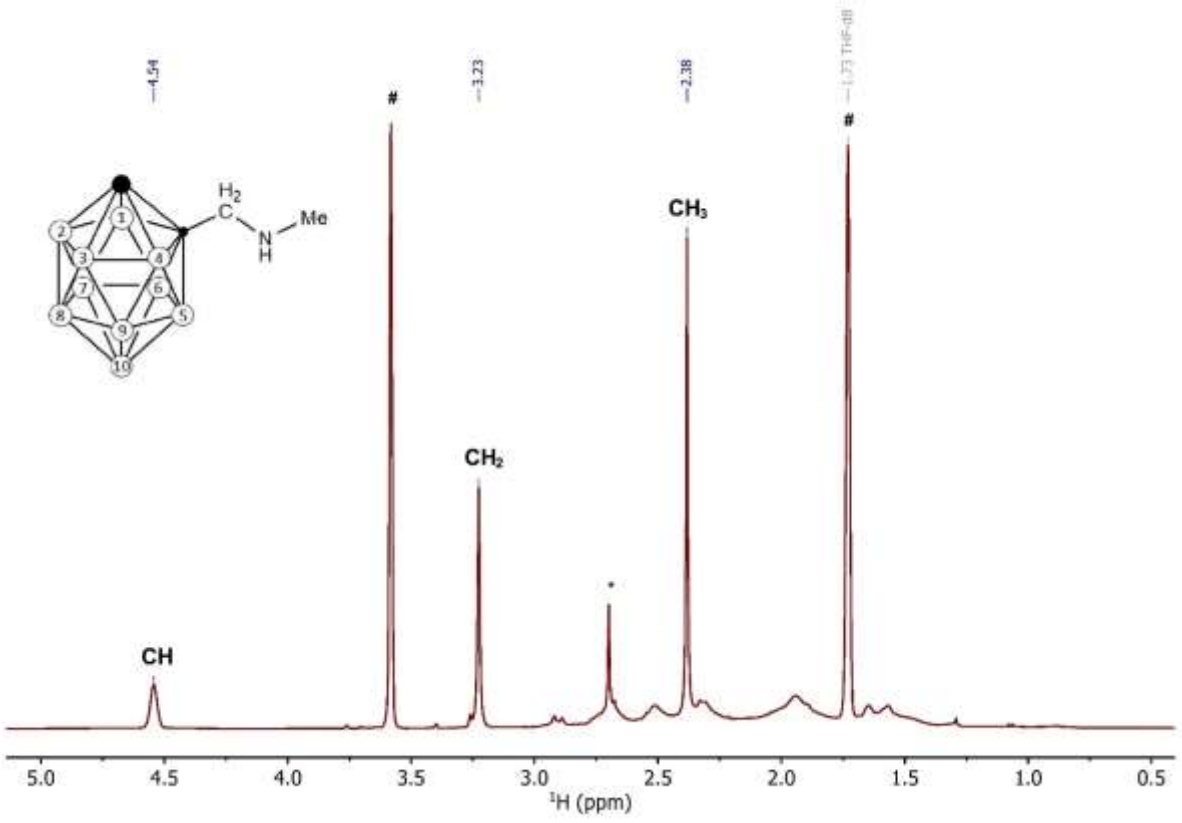

Figure S22. 400.3 MHz ^{1}H NMR spectrum of **3** in THF-d_8. Residual solvent signals are marked with #. The signal marked with * is from an impurity.

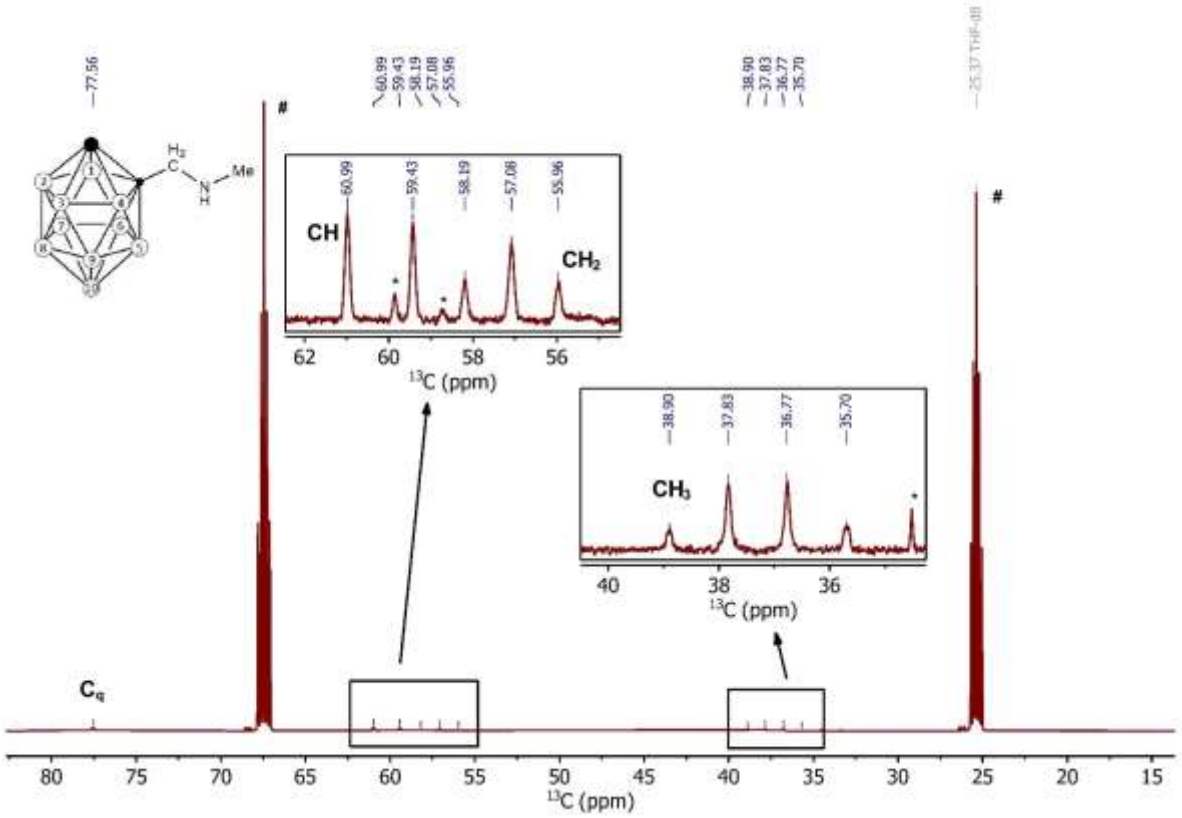

Figure S23. 125.8 MHz proton coupled ^{13}C NMR spectrum of **3** in THF-d_8. Solvent signals are marked with #. Signals marked with * are from impurities.

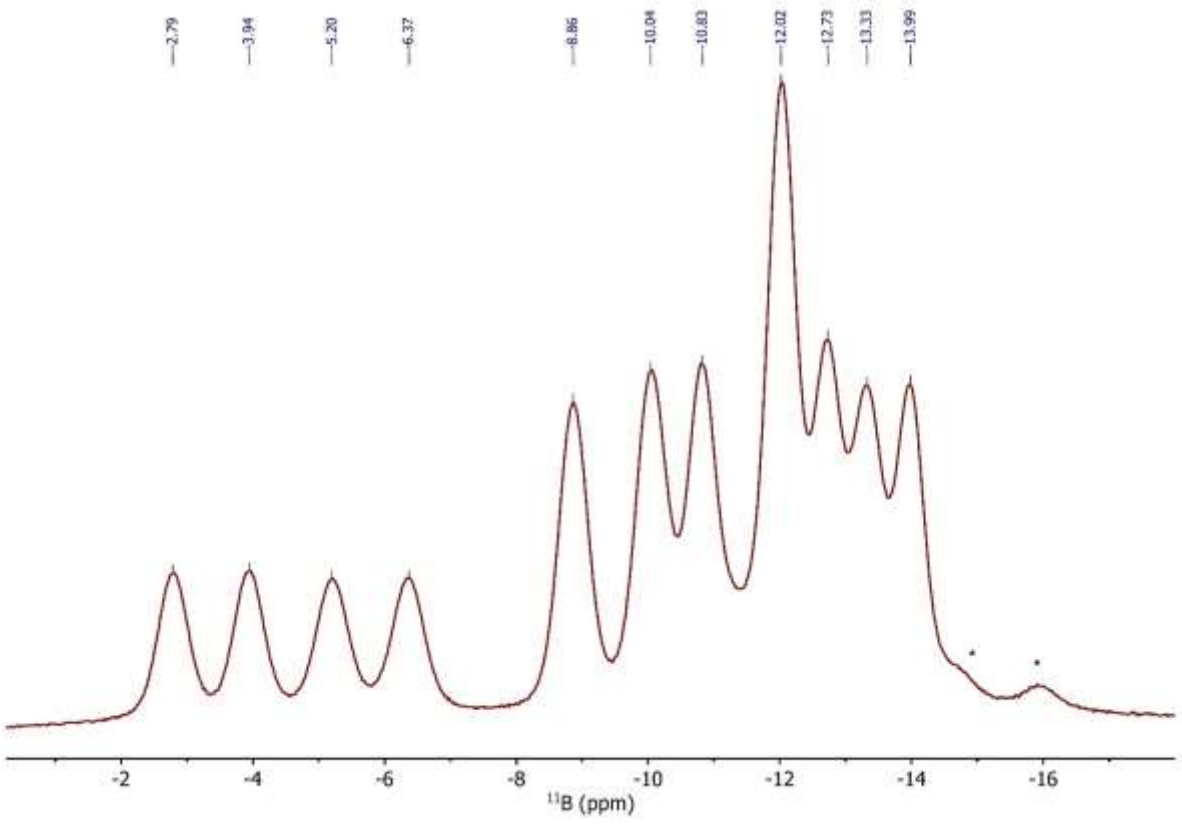

Figure S24. 128.4 MHz ^{11}B NMR spectrum of **3** in THF-d_8. Signals marked with * are from impurities.

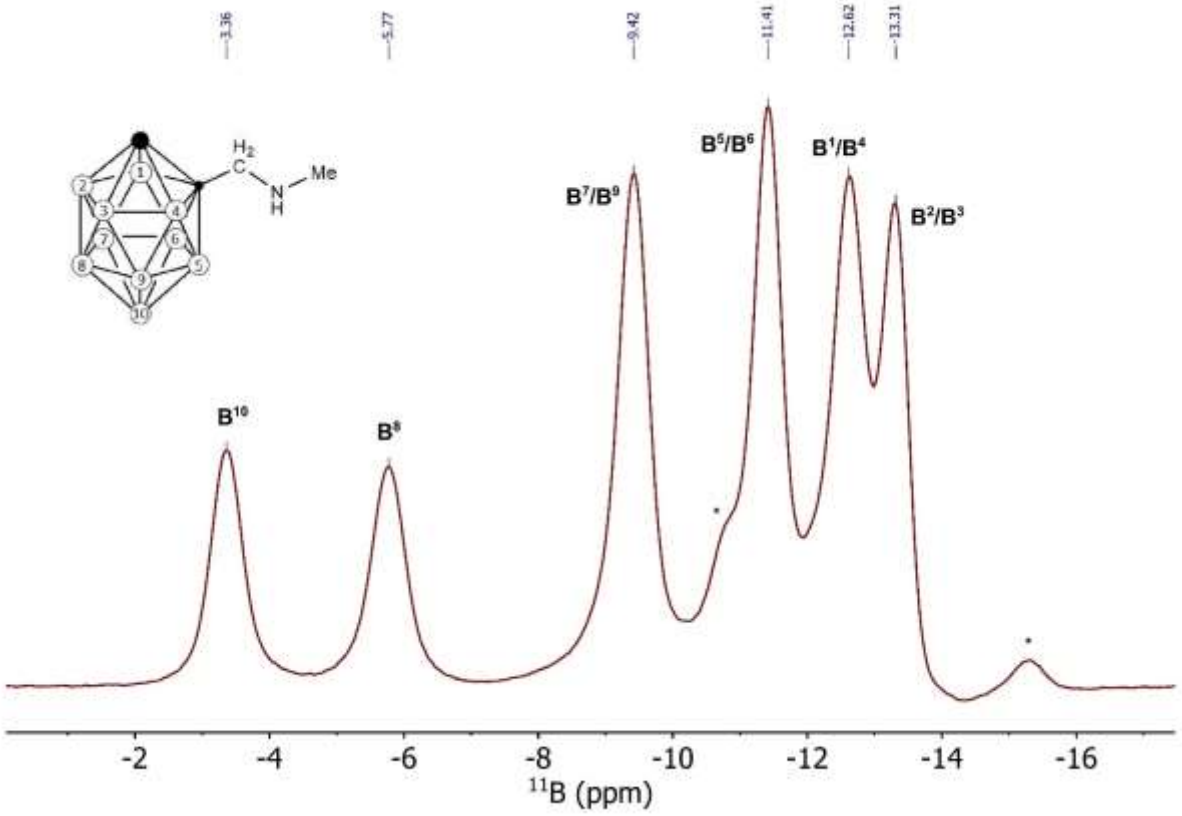

Figure S25. 128.4 MHz $^{11}B\{^{1}H\}$ NMR spectrum of **3** in THF-d_8. Signals marked with * are from impurities.

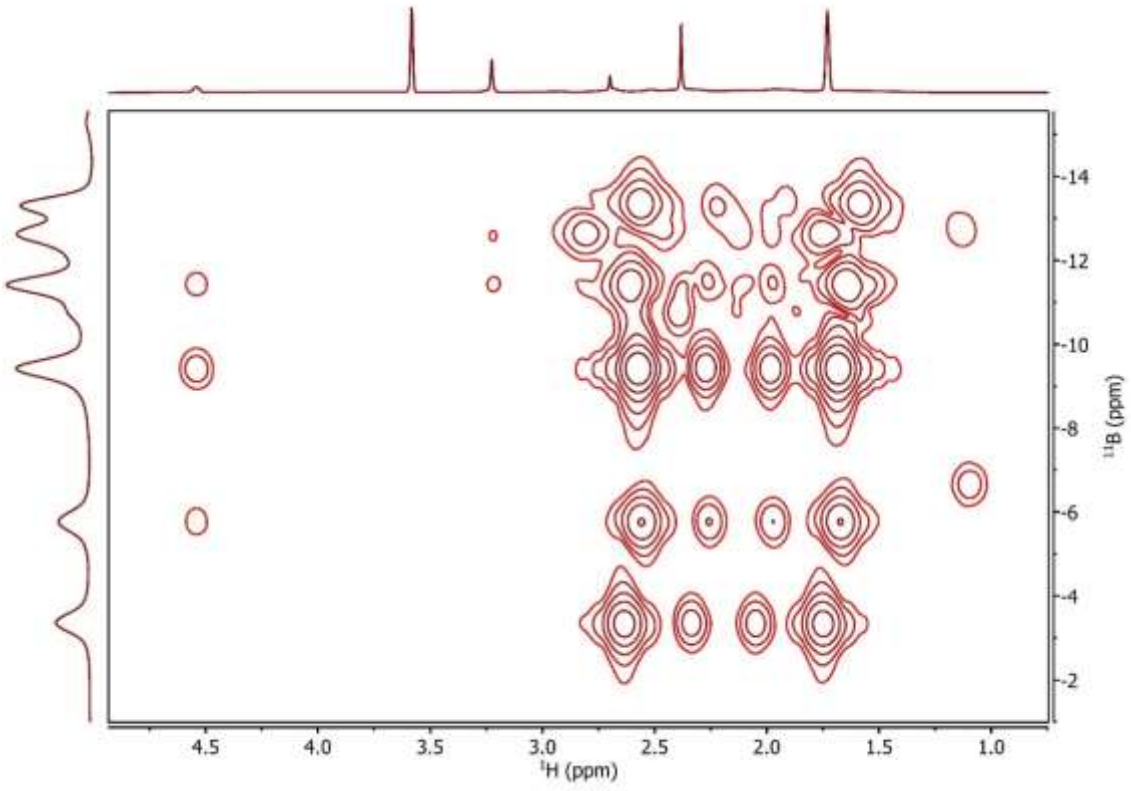

Figure S26. $^{1}H,^{11}B$ HMQC spectrum (^{1}H = 500.3 MHz) of **3** in THF-d_8.

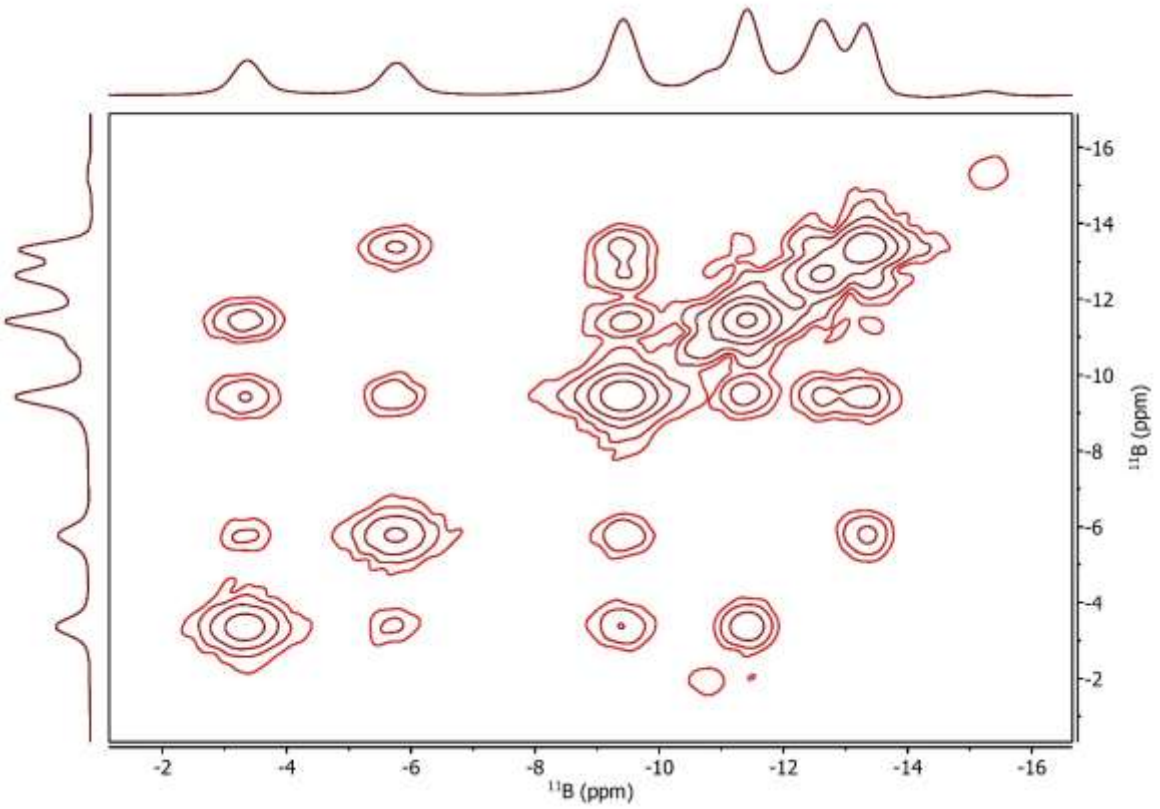

Figure S27. 128.4 MHz $^{11}B\{^{1}H\}$ COSY spectrum of **3** in THF-d_8.

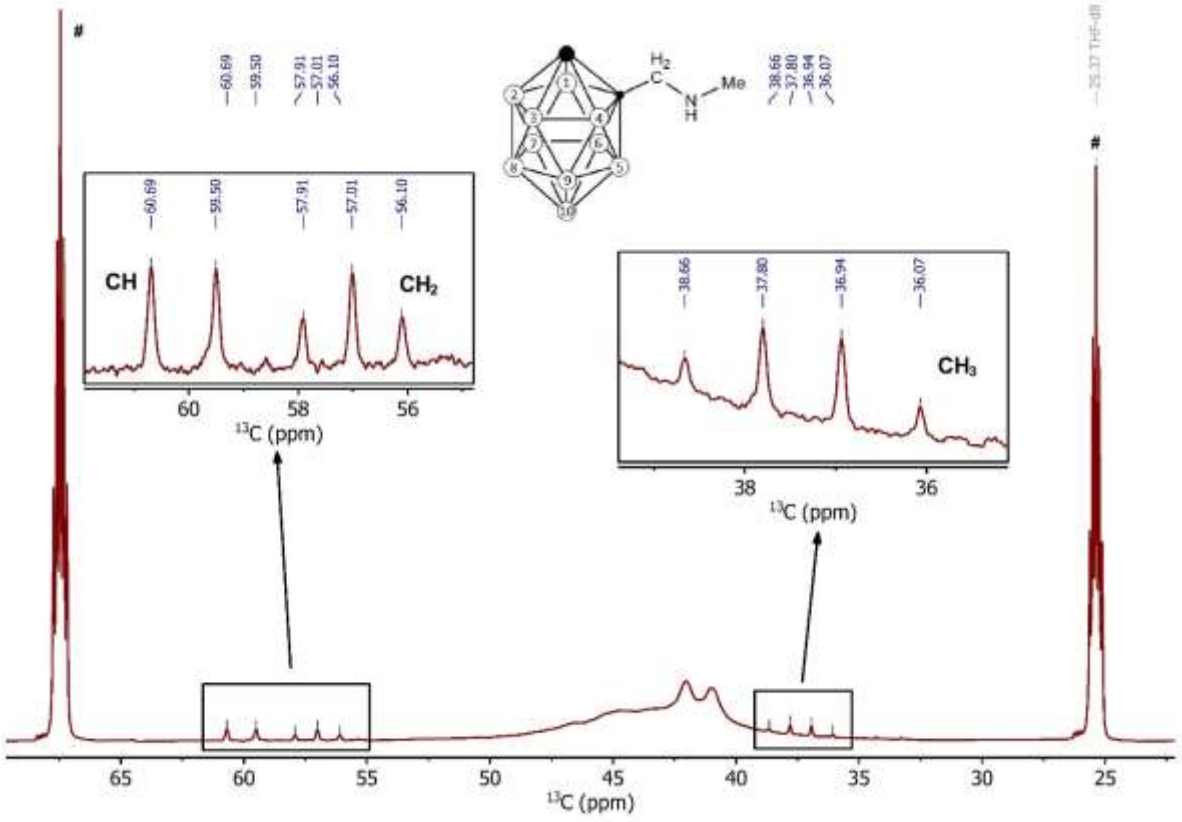

Figure S28. 150.9 MHz proton coupled ^{13}C NMR spectrum of **3** in PS/THF-d_8 after 15 days of swelling. Solvent signals are marked with #. The broad signals between 40 and 50 ppm belong to the aliphatic carbons of polystyrene.

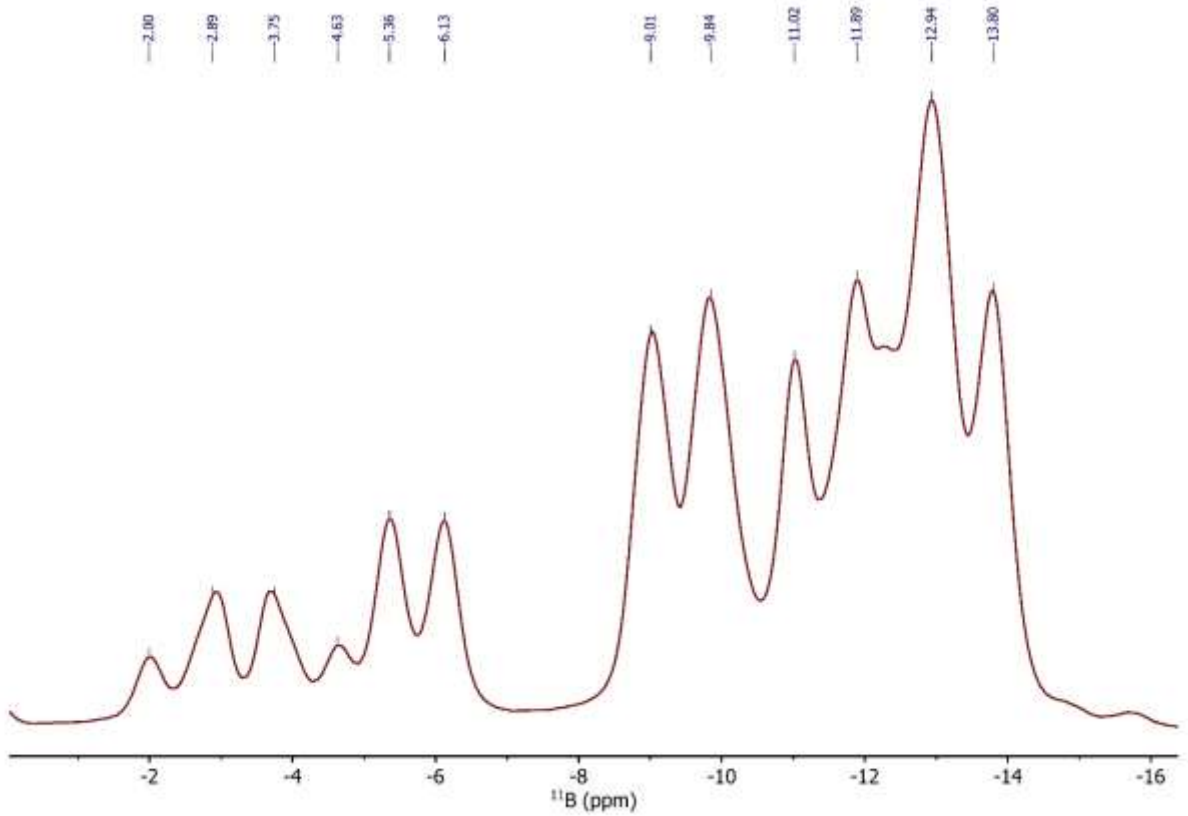

Figure S29. 192.6 MHz ^{11}B NMR spectrum of **3** in PS/THF-d_8 after 15 days of swelling.

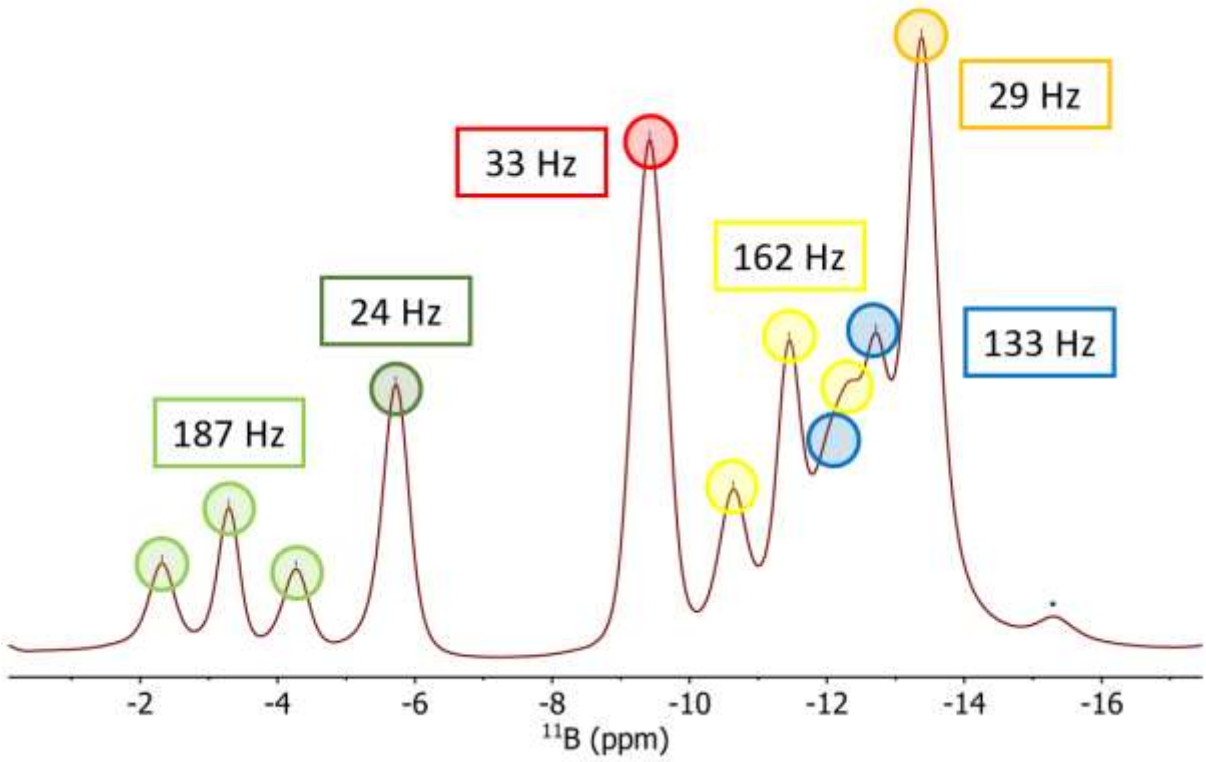

Figure S30. 192.6 MHz ^{11}B{^{1}H} NMR spectrum of **3** in PS/THF-d_8 after 15 days of swelling. The signal marked with * results from an impurity. The quadrupolar triplets are marked in different colours and labelled with absolute ^{11}B RQC values.

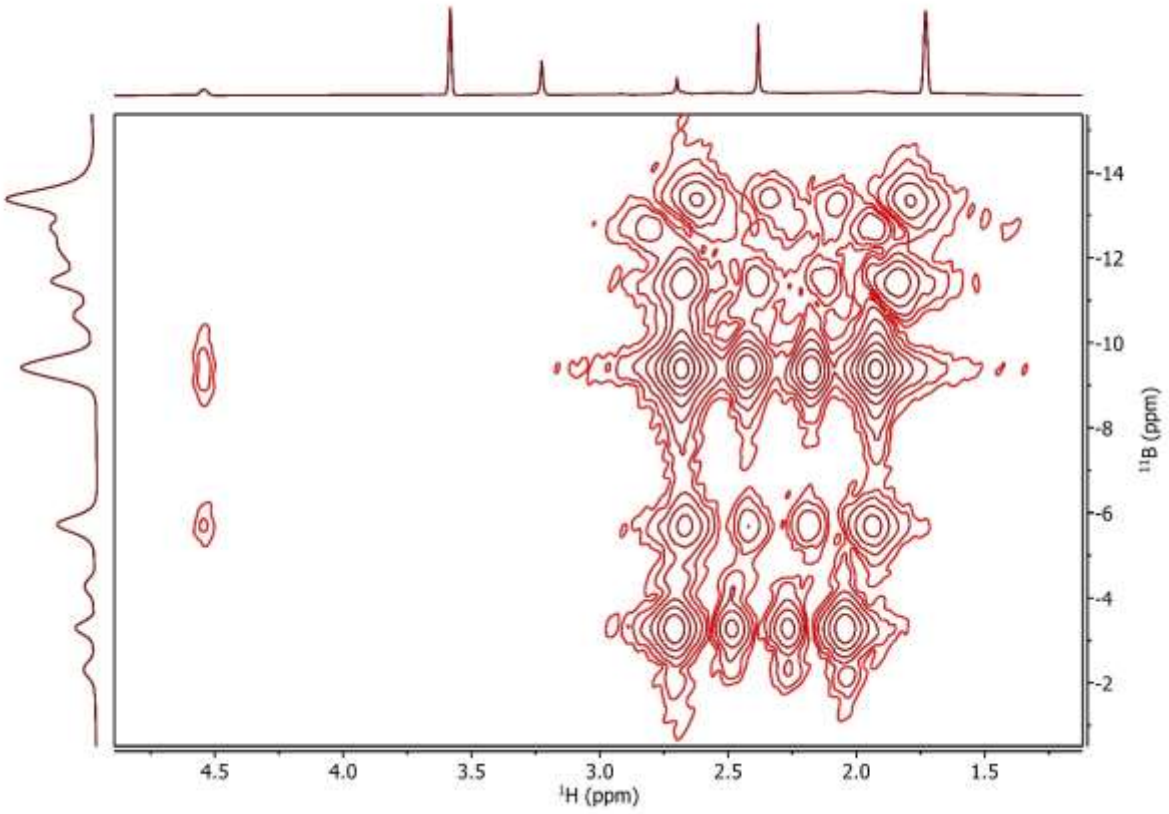

Figure S31. ^{1}H,^{11}B HMQC spectrum (^{1}H = 600.3 MHz, 90° ^{11}B flip angle) of **3** in PS/THF-d_8 after 15 days of swelling. The horizontal trace is taken from the isotropic ^{1}H 1D spectrum.

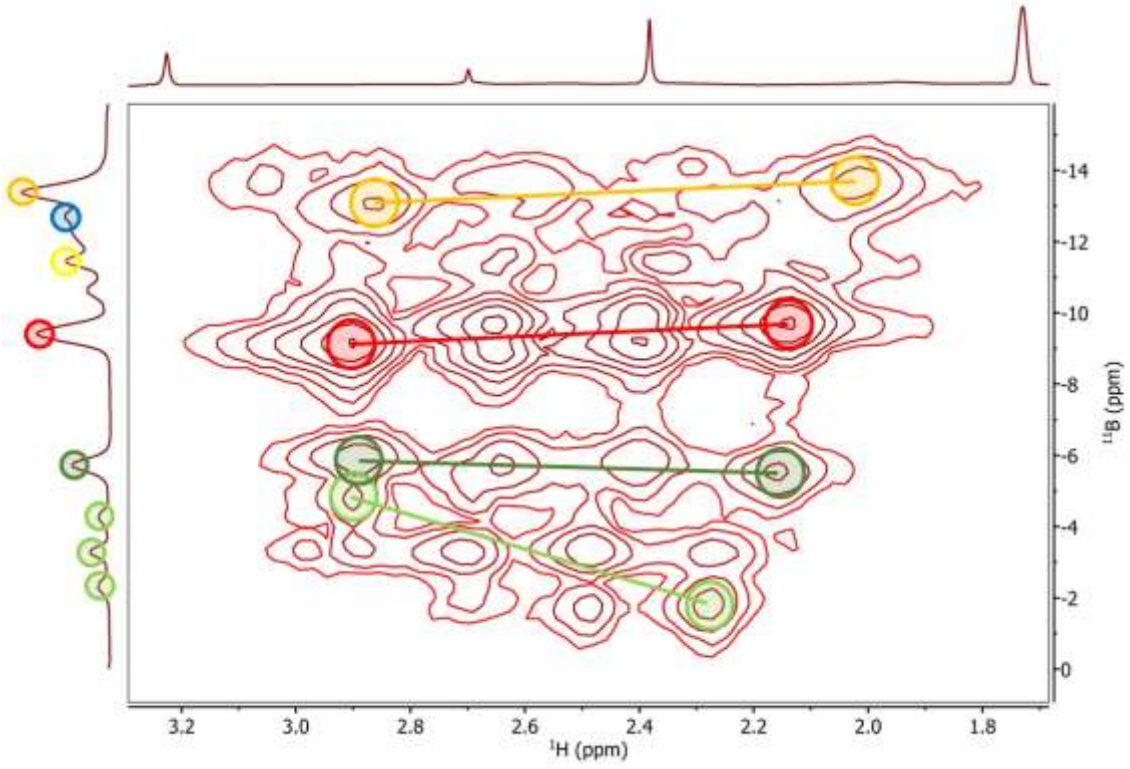

Figure S32. ^{1}H,^{11}B HMQC spectrum (^{1}H = 600.3 MHz, 45° ^{11}B flip angle) of **3** in PS/THF-d_8 after 15 days of swelling. The correlations that are crucial for the ^{11}B RQC sign determination are marked in the same colours as in **Figure S30**. The signal marked in dark green shows a slight negative tilt with an ^{11}B RQC of −24 Hz while the signals marked in red and orange show a slight positive tilt with ^{11}B RQCs of 33 and 29 Hz, respectively.

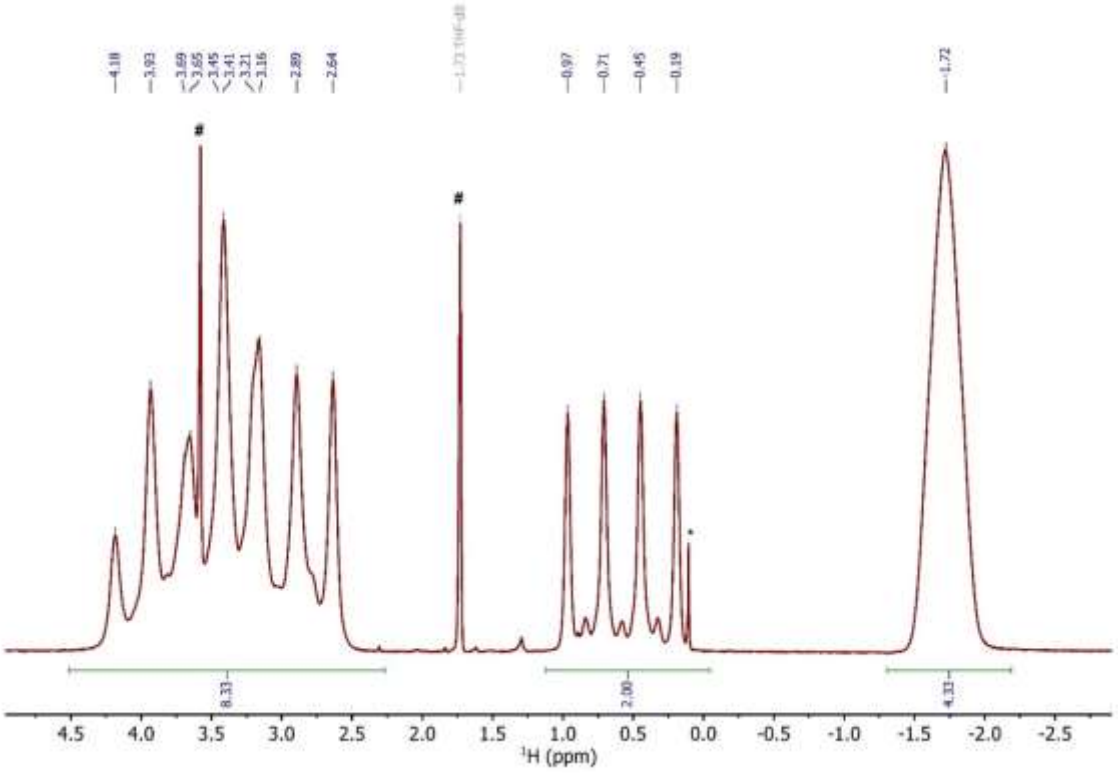

Figure S33. 600.3 MHz ^{1}H NMR spectrum of **4** in THF-d_8. Residual solvent signals are marked with #. The signal marked with * is caused by an impurity.

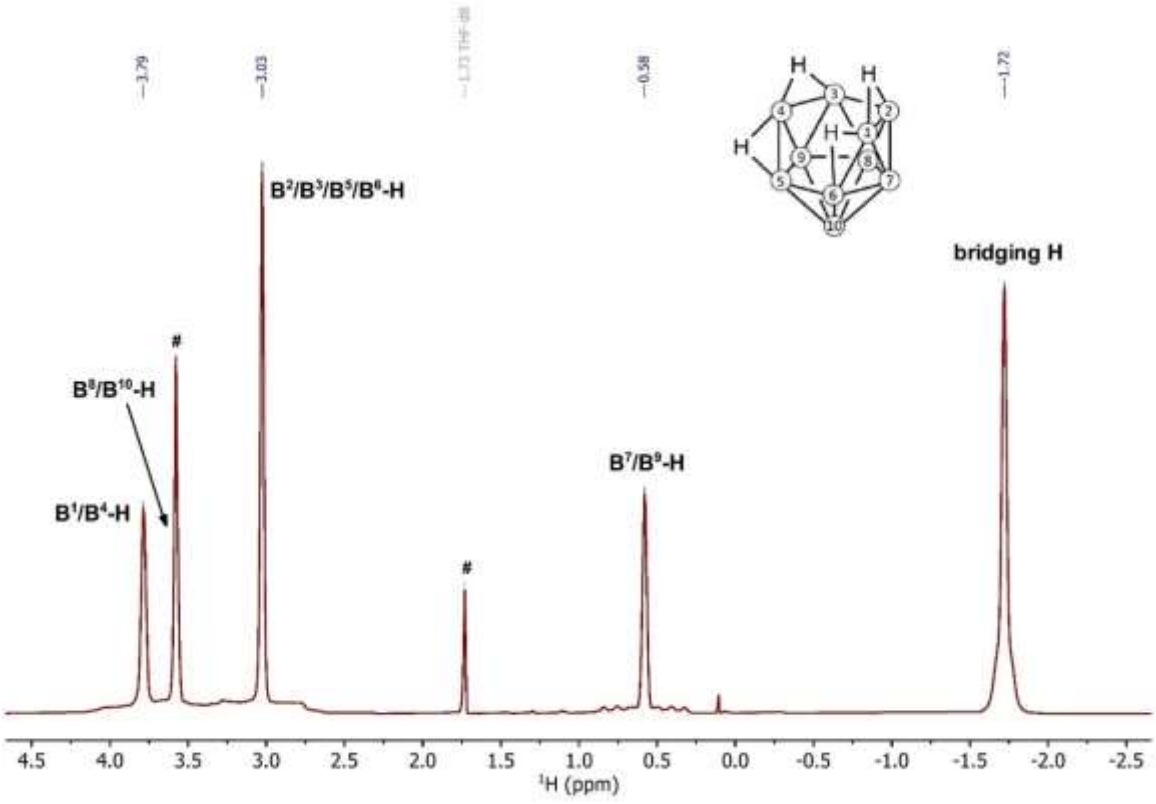

Figure S34. 600.3 MHz $^{1}H\{^{11}B\}$ NMR spectrum of **4** in THF-d_8. Residual solvent signals are marked with #.

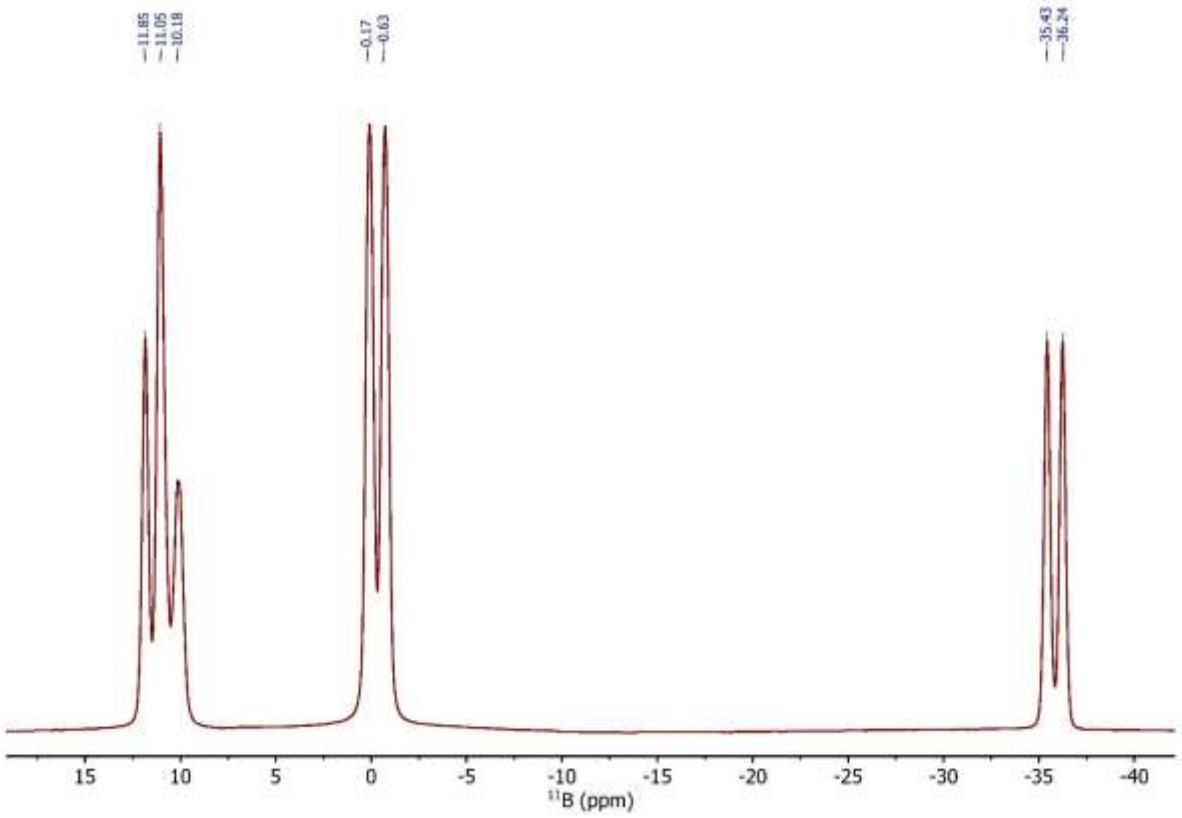

Figure S35. 192.6 MHz ^{11}B NMR spectrum of **4** in THF-d_8.

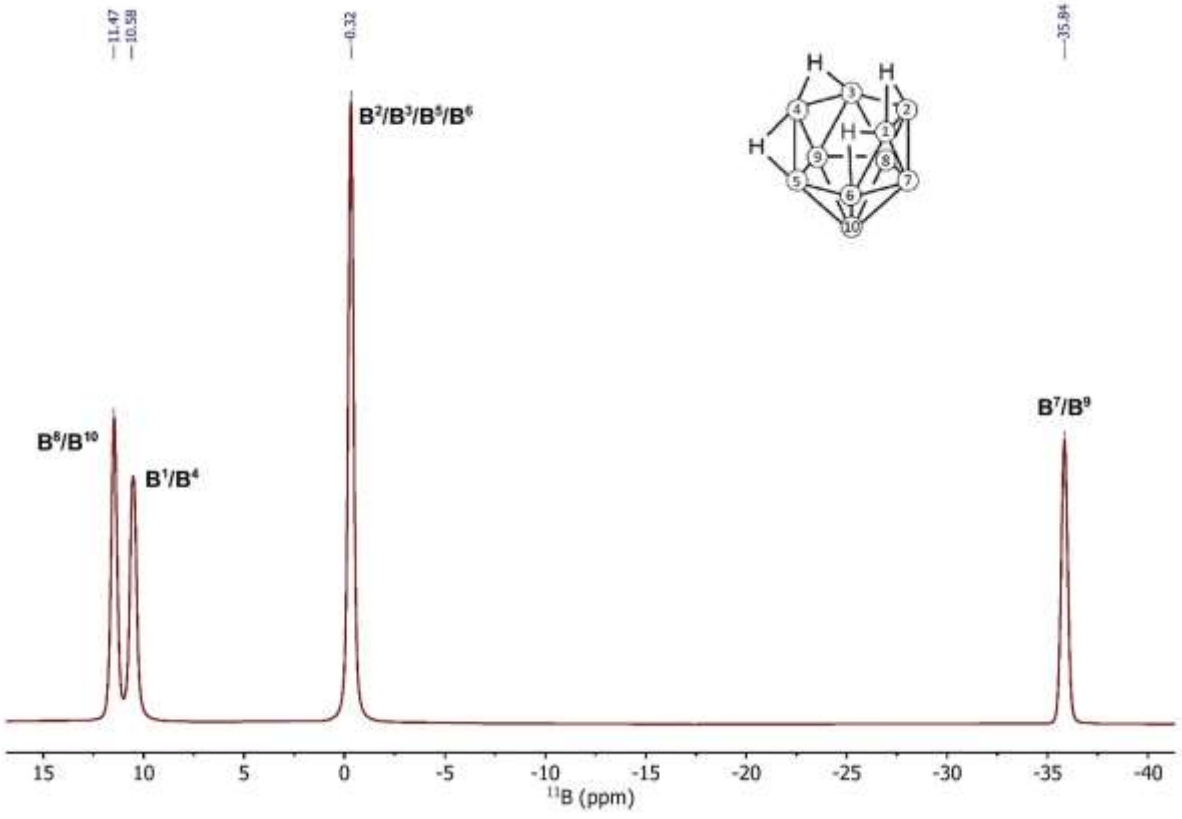

Figure S36. 192.6 MHz ^{11}B{^{1}H} NMR spectrum of **4** in THF-d_8.

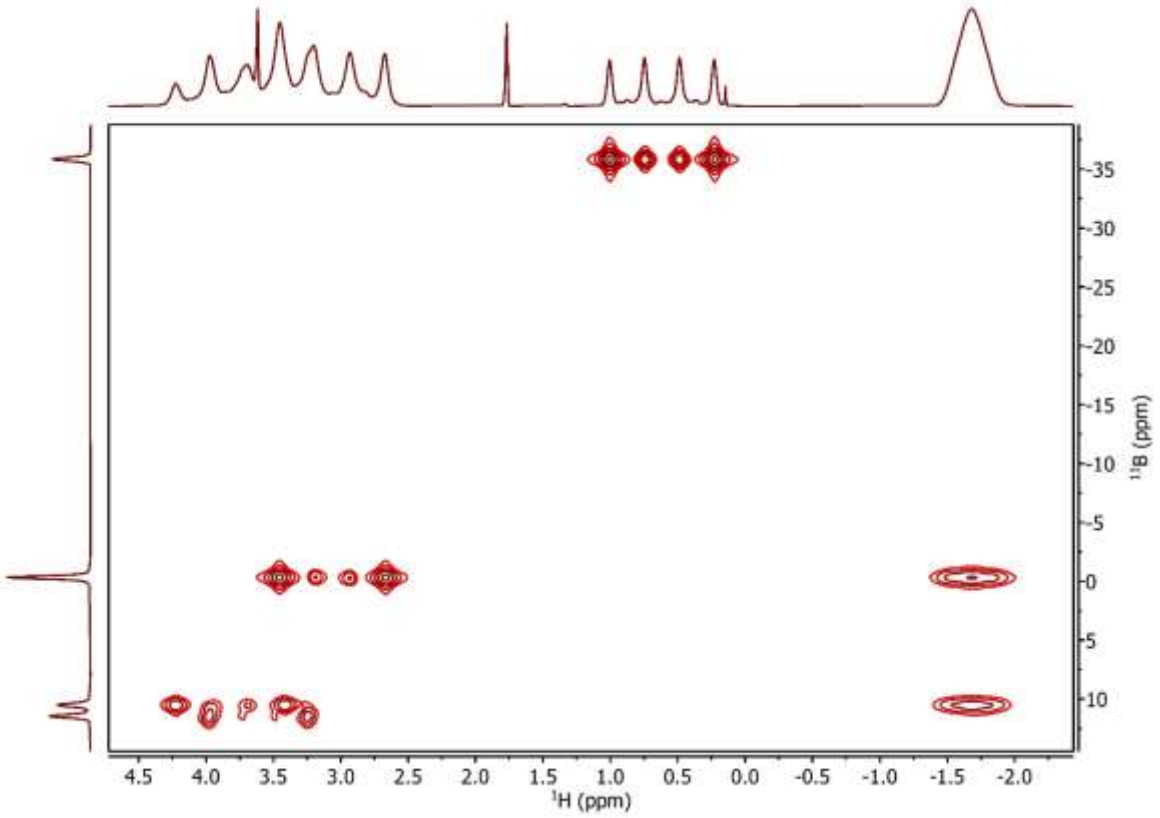

Figure S37. ^{1}H,^{11}B HMQC spectrum (^{1}H = 600.3 MHz) of **4** in THF-d_8.

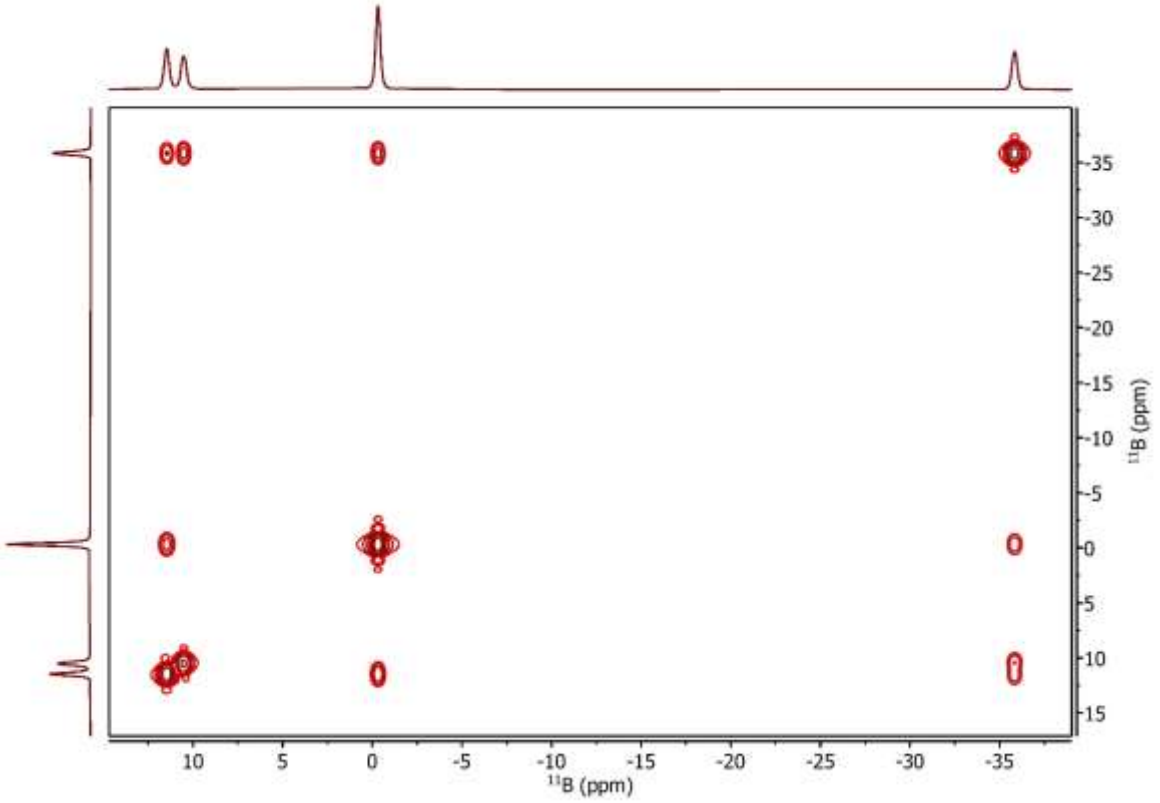

Figure S38. 192.6 MHz ^{11}B{^{1}H} COSY spectrum of **4** in THF-d_8.

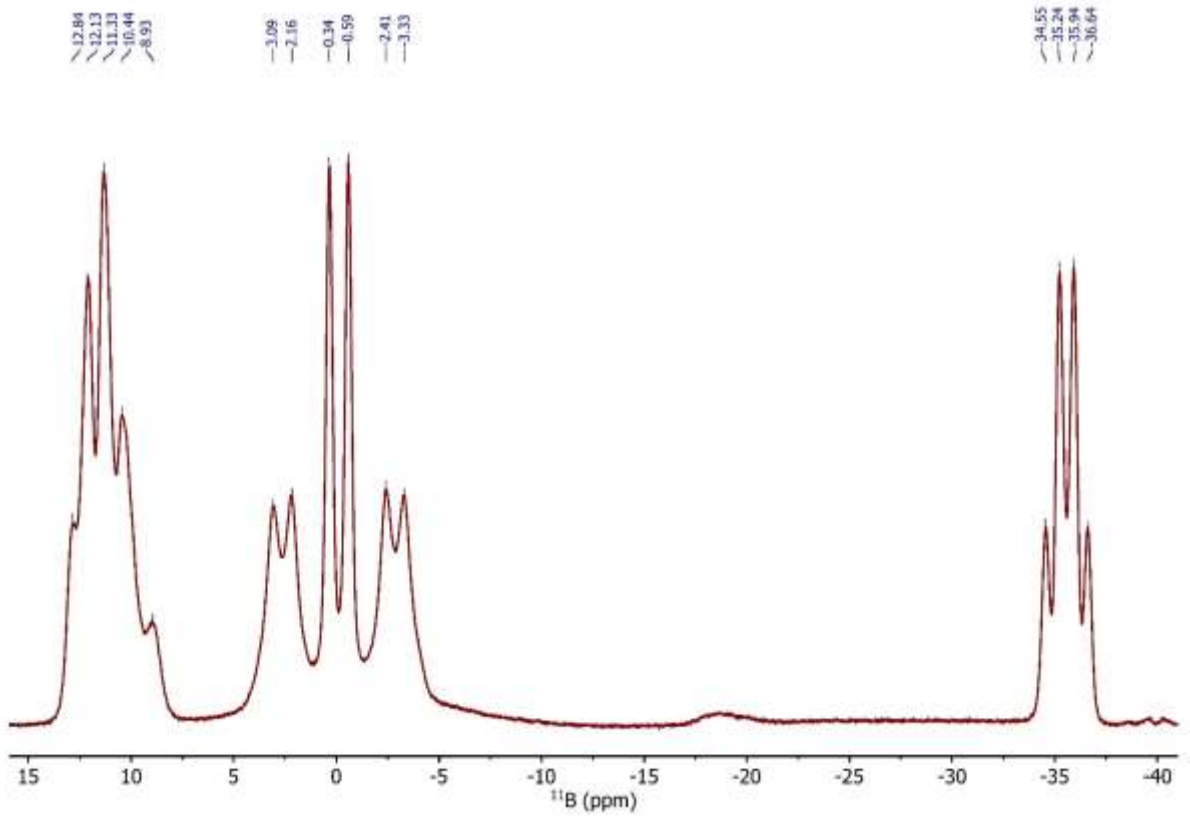

Figure S39. 192.6 MHz ^{11}B NMR spectrum of **4** in PS/THF-d_8 after 11 days of swelling.

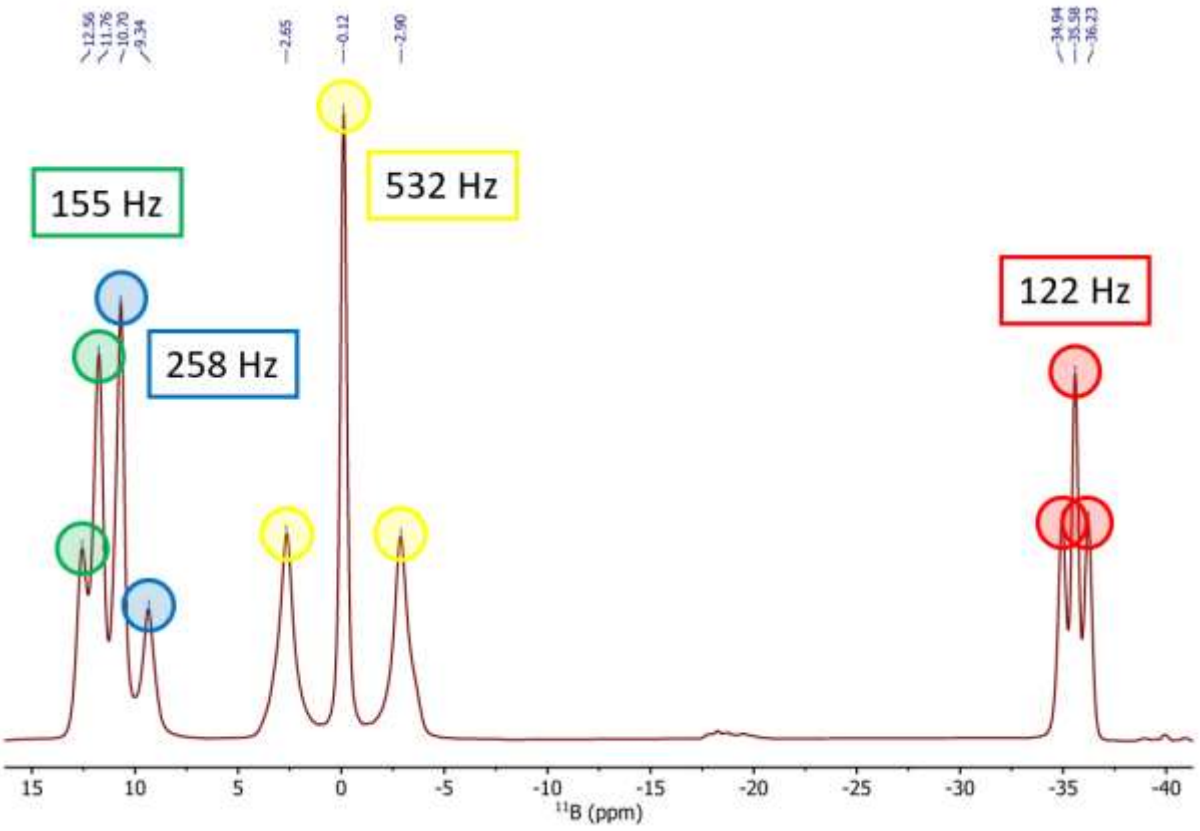

Figure S40. 192.6 MHz ^{11}B{^{1}H} NMR spectrum of **4** in PS/THF-d_8 after 11 days of swelling. The quadrupolar triplets are marked in different colours and labelled with absolute ^{11}B RQC values.

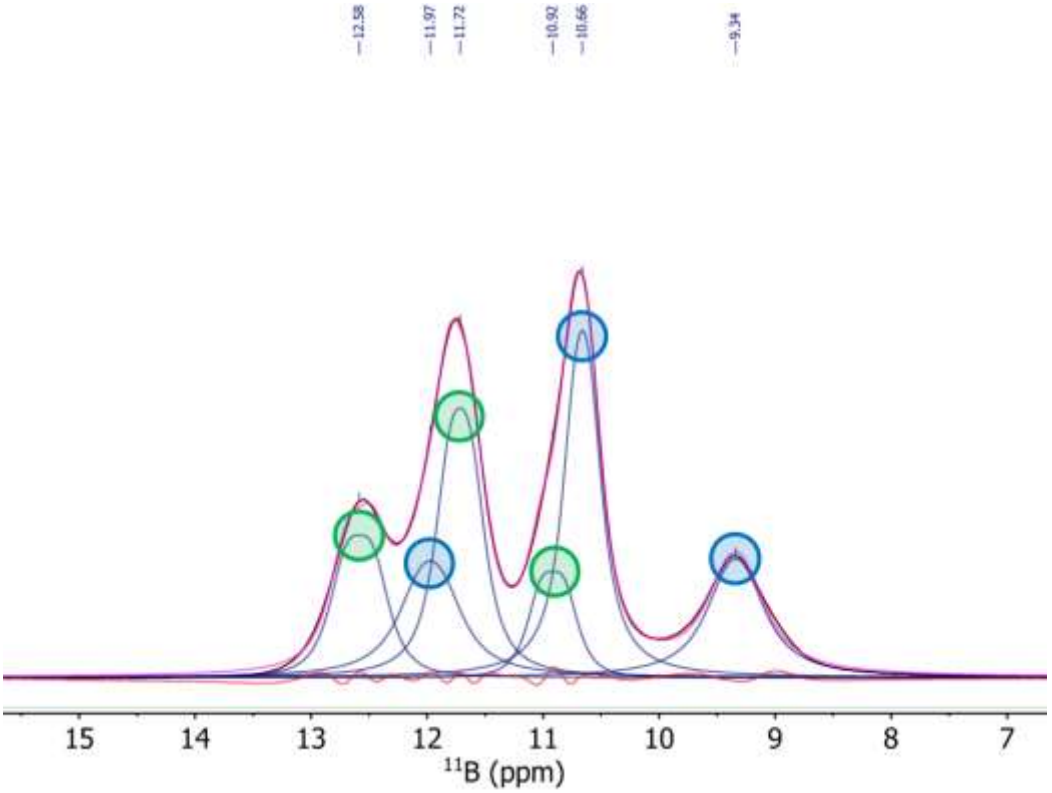

Figure S41. Excerpt of a 192.6 MHz $^{11}B\{^{1}H\}$ NMR spectrum of **4** in PS/THF-d_8 after 11 days of swelling showing the two overlapped signals marked in green and blue. A lineshape fitting analysis shows the two overlapped satellite transitions hidden beneath the two central transitions of the signals.

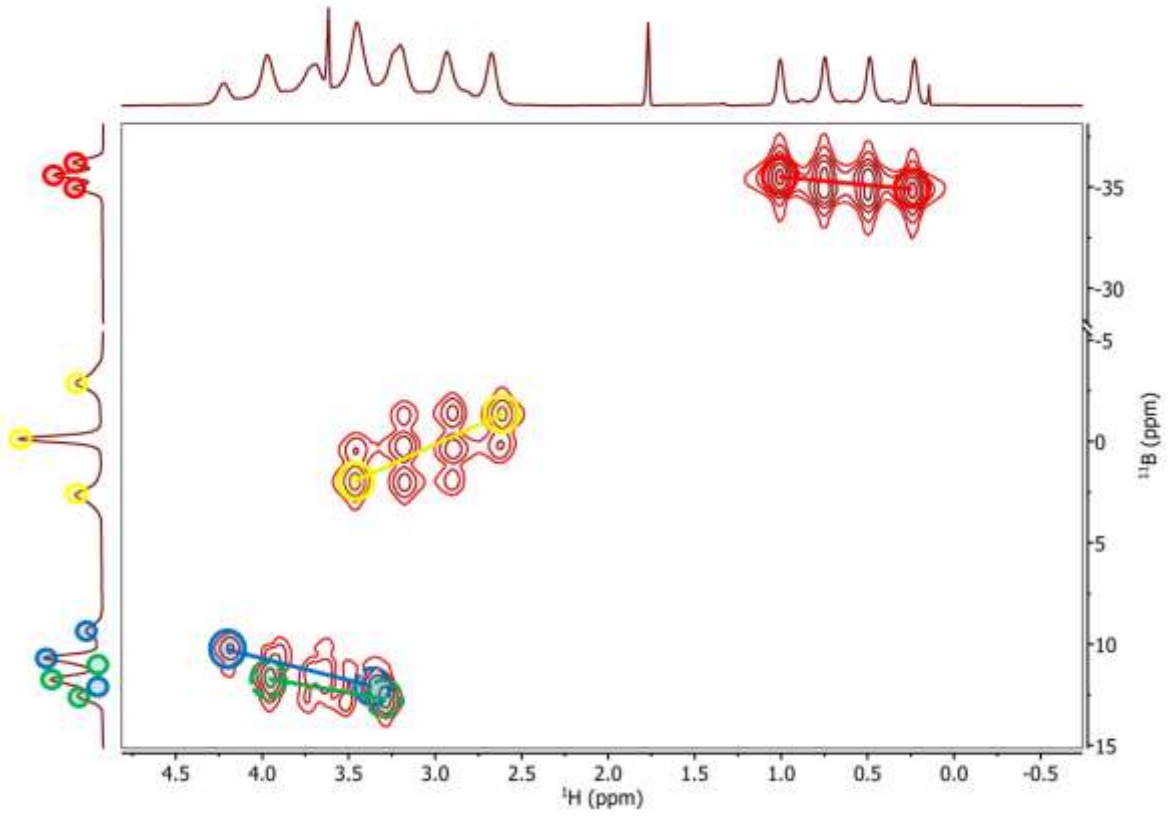

Figure S42. $^{1}H,^{11}B$ HMQC spectrum (^{1}H = 600.3 MHz, 45° ^{11}B flip angle) of **4** in PS/THF-d_8 after 11 days of swelling. The ^{1}H 1D trace is taken from the isotropic spectrum. The correlations that are crucial for the ^{11}B RQC sign determination are marked in the same colours as in **Figure S40**. The dashed circles mark overlapped satellite transitions. The region between –5 ppm and –30 ppm in the ^{11}B dimension has been cut out for clarity.

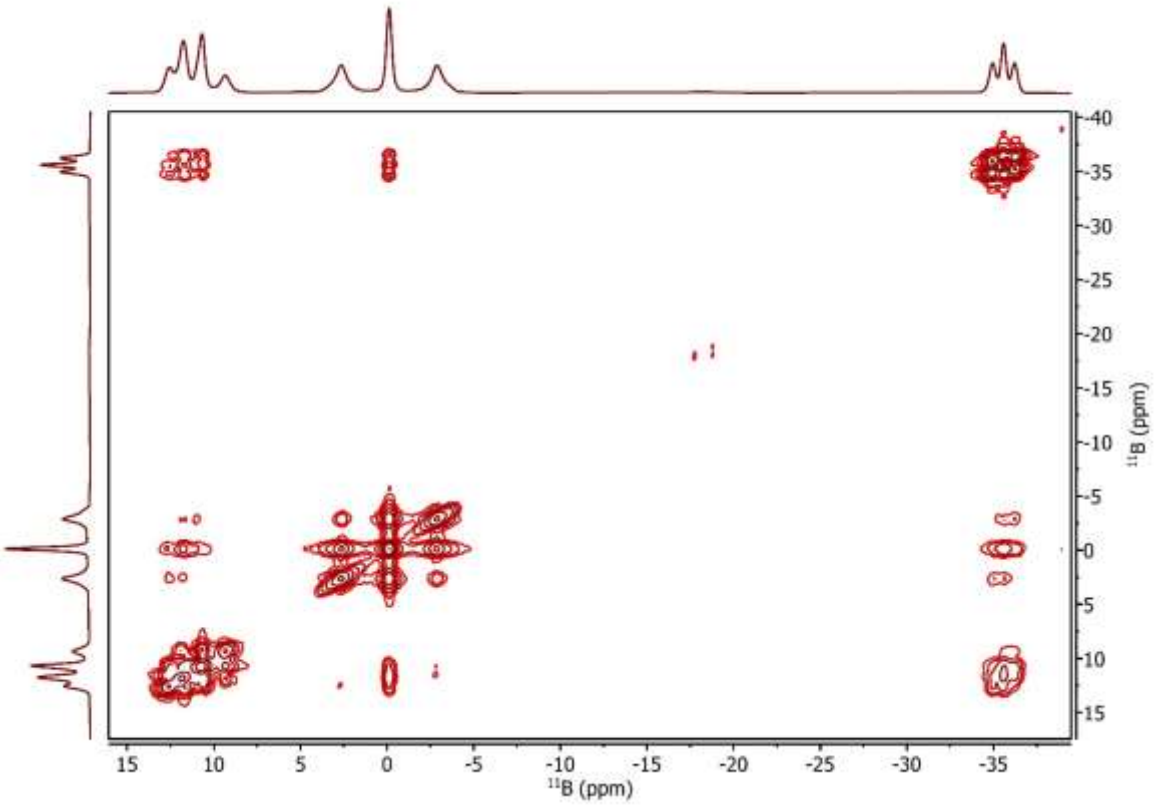

Figure S43. 192.6 MHz $^{11}B\{^{1}H\}$ COSY spectrum of **4** in PS/THF-d_8 after 11 days of swelling.

Experimental Anisotropic NMR Parameters

Table S1. Experimentally determined ^{11}B-^{1}H RDCs, ^{13}C-^{1}H RDCs and ^{11}B RQCs for **1** - **4**.

	1	**2**	**3**	**4**
B^1, B^4 B-H RDC / RQC [Hz]	2.8 / −642	8.4 / 274	−1.6 / −133	8.8 / −258
B^2, B^3 B-H RDC / RQC [Hz][a)]	15.8 / 440	10.2 / −25[c)]	2.4 / 29[c)]	21.5 / 532
B^5, B^6 B-H RDC / RQC [Hz][a)]	15.8 / 440	10.2 / −25[c)]	6.8 / 162	21.5 / 532
B^7, B^9 B-H RDC / RQC [Hz]	19.2 / 285	−31.3 / −533	3.3 / 33[c)]	−3.7 / −122
B^8 B-H RDC / RQC [Hz][a)]	−33.7 / −540	11.2 / 125	−1.5 / −24[c)]	−22.3 / −155
B^{10} B-H RDC / RQC [Hz][a)]	−33.7 / −540	11.2 / 125	−14.5 / −187	−22.3 / −155
C-H RDC [Hz]	−42.1	−31.4	−16.3[b)]	-

a) In case of **1, 2** and **4**, B^2 ,B^3 ,B^5 and B^6 and B^8 and B^{10} are chemically equal, respectively.

b) In case of **3**, the C-H RDC of C^{11}-H, where C^{11} is part of the icosahedron, is given.

c) In these cases, the magnitude of the RQC was estimated from the tilt (frequency difference between the outer signals of the quartet divided by 2) and extrapolated to the magnitude of alignment present in the sample used for the signal assignment procedure.

RDCs were measured with an error of ca. 1 Hz, RQCs with an error of ca. 5 Hz.

Graphical representation of alignment tensors

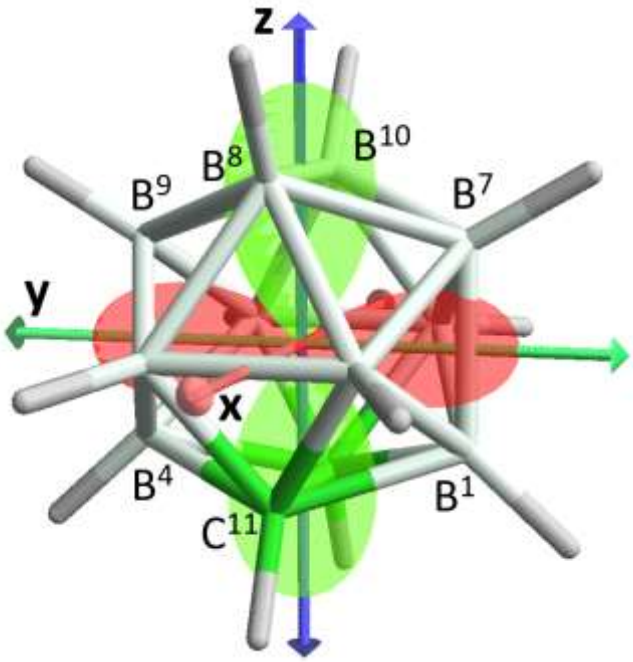

Figure S44. Graphical representation of the alignment tensor of **1** determined from ^{13}C-^{1}H and ^{11}B-^{1}H RDCs. The axes correspond to the eigensystem of **A** following the convention $|A_{zz}|>|A_{yy}|>|A_{xx}|$ with the eigenvalues shown in **Table S2**. The green lobes indicate a positive sign and thus the orientation along this direction is more favored than in isotropic solution. The red lobe represents directions of negative alignment along which the orientation is less favored than in isotropic solution.

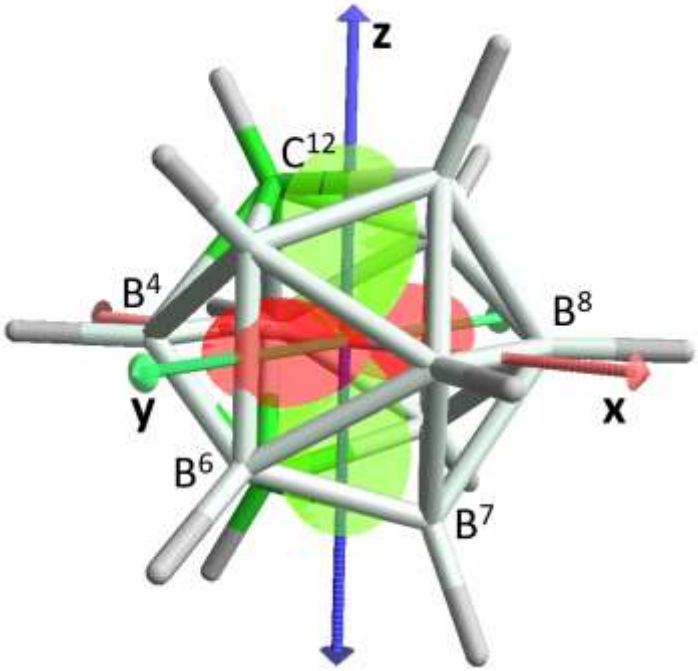

Figure S45. Graphical representation of the alignment tensor of **2** determined from ^{13}C-^{1}H and ^{11}B-^{1}H RDCs. The axes correspond to the eigensystem of **A** following the convention $|A_{zz}|>|A_{yy}|>|A_{xx}|$ with the eigenvalues shown in **Table S2**. Colour coding is analogous to **Figure S44**.

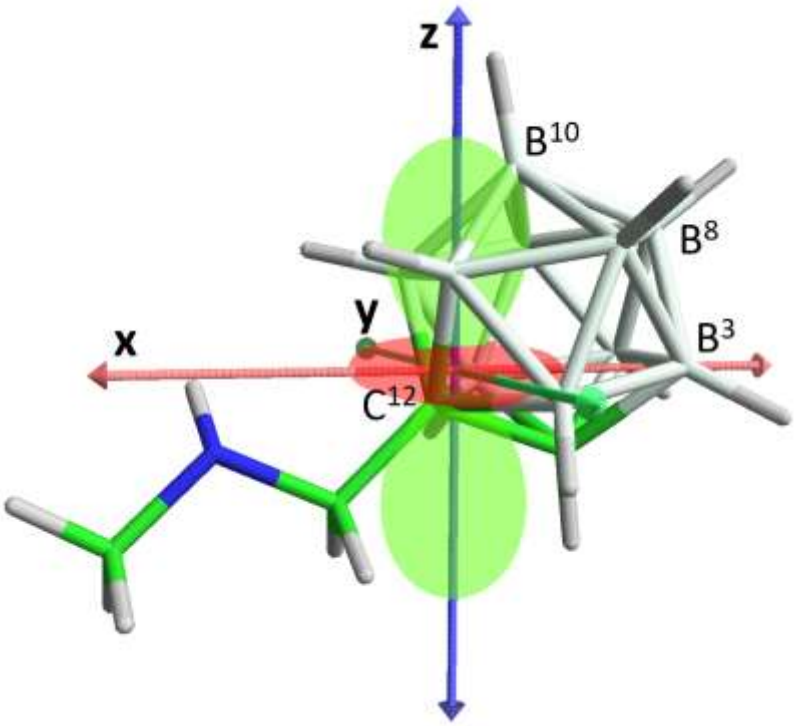

Figure S46. Graphical representation of the alignment tensor of **3** determined from ^{13}C-^{1}H and ^{11}B-^{1}H RDCs. The axes correspond to the eigensystem of **A** following the convention $|A_{zz}|>|A_{yy}|>|A_{xx}|$ with the eigenvalues shown in **Table S2**. Colour coding is analogous to **Figure S44**.

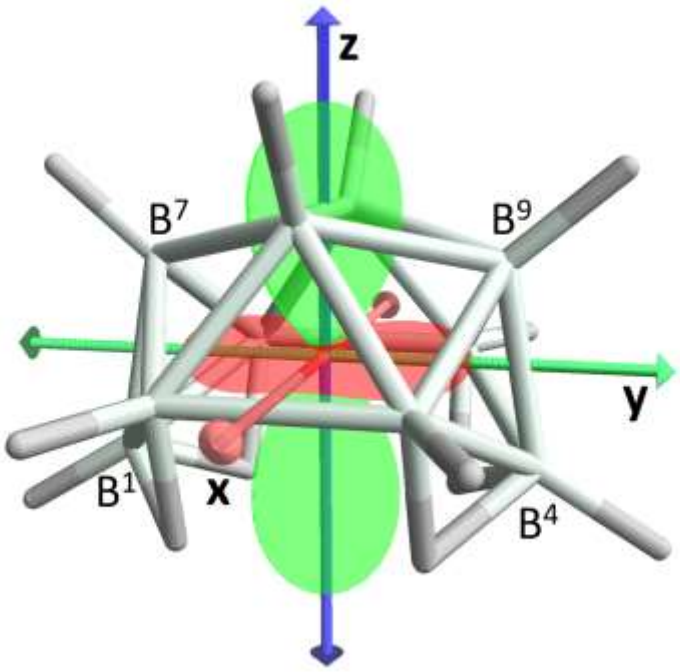

Figure S47. Graphical representation of the alignment tensor of **4** determined from ^{11}B-^{1}H RDCs. The axes correspond to the eigensystem of **A** following the convention $|A_{zz}|>|A_{yy}|>|A_{xx}|$ with the eigenvalues shown in **Table S2**. Colour coding is analogous to **Figure S44**.

DFT geometry optimized structure models and graphical representation of EFG tensors

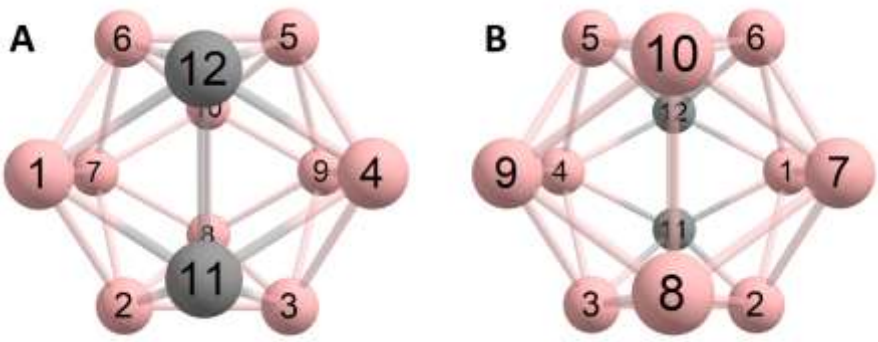

Figure S48. Top (**A**) and bottom (**B**) view of a structure model of **1**, geometry optimized at the B3LYP/Def2TZVP level of theory. The positions are numbered for NMR signal assignment and discussion of EFG tensors. Hydrogen atoms are omitted for clarity.

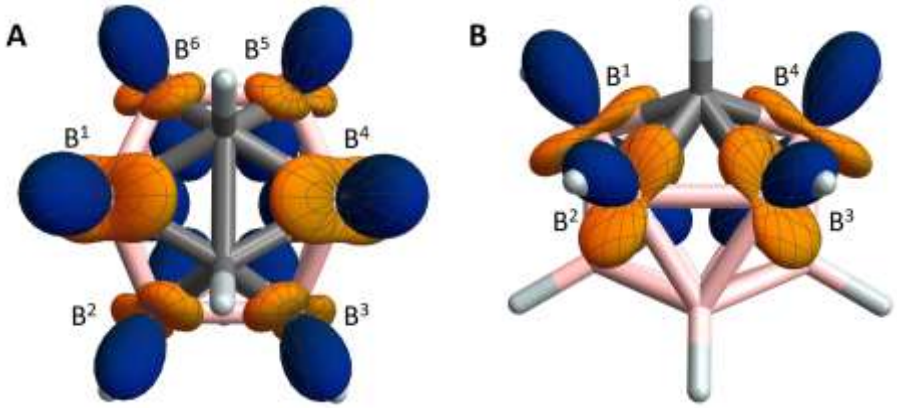

Figure S49. Top (**A**) and side (**B**) view onto a structure model of **1** with the EFG tensors shown at the boron positions 1-6. The blue and orange lobes indicate positive and negative signs for the EFG, respectively. The EFG tensor is given in the Gaussian sign convention which is opposite to the more commonly used sign convention used by Autschbach *et. al.*[5]

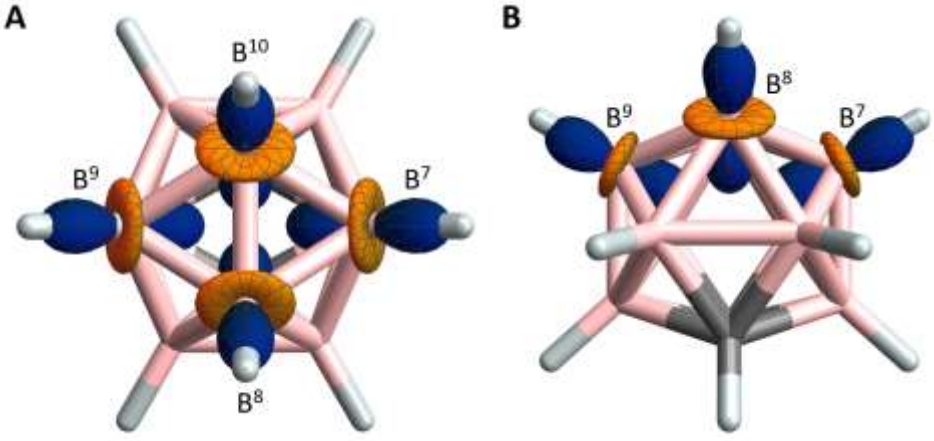

Figure S50. Top (**A**) and side (**B**) view onto a structure model of **1** with the EFG tensors shown at the boron positions 7-10. Colour coding and sign convention in analogous to **Figure S49**.

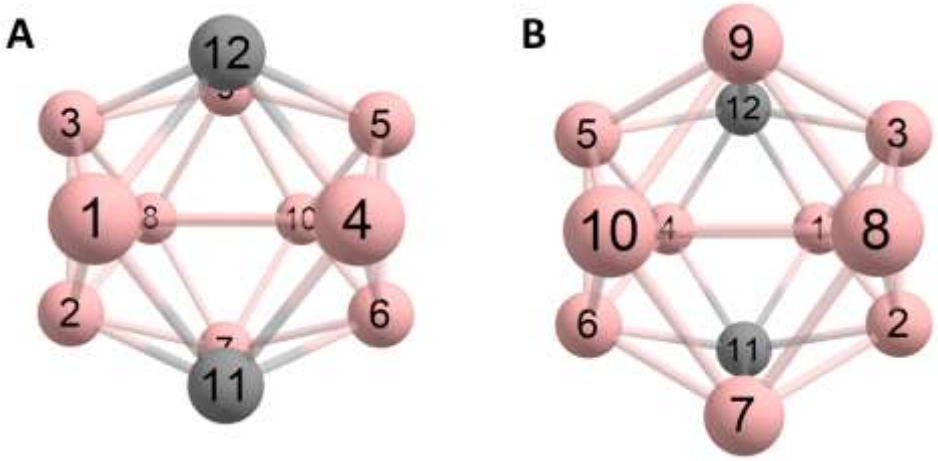

Figure S51. Top (**A**) and bottom (**B**) view of a structure model of **2**, geometry optimized at the B3LYP/Def2TZVP level of theory. The positions are numbered for NMR signal assignment and discussion of EFG tensors. Hydrogen atoms are omitted for clarity.

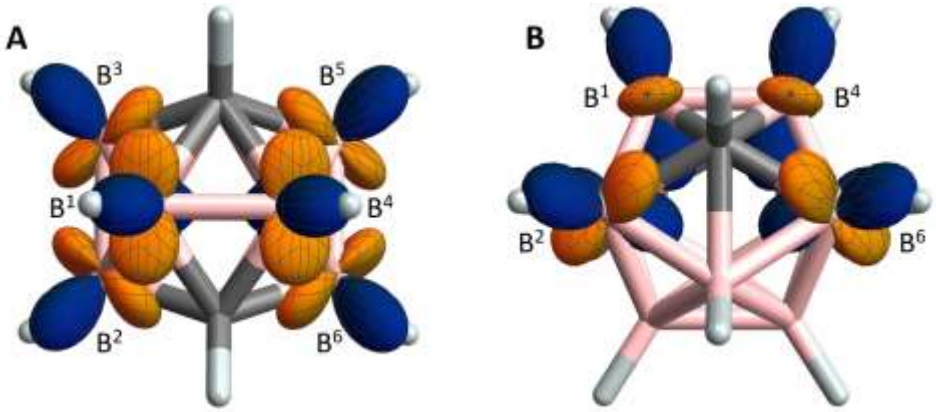

Figure S52. Top (**A**) and side (**B**) view onto a structure model of **2** with the EFG tensors shown at the boron positions 1-6. Colour coding and sign convention is analogous to **Figure S49**.

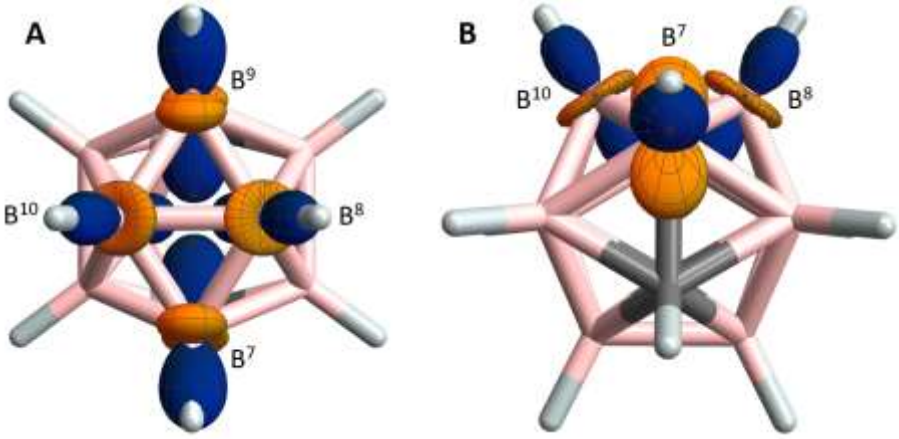

Figure S53. Top (**A**) and side (**B**) view onto a structure model of **2** with the EFG tensors shown at the boron positions 7-10. Colour coding and sign convention is analogous to **Figure S49**.

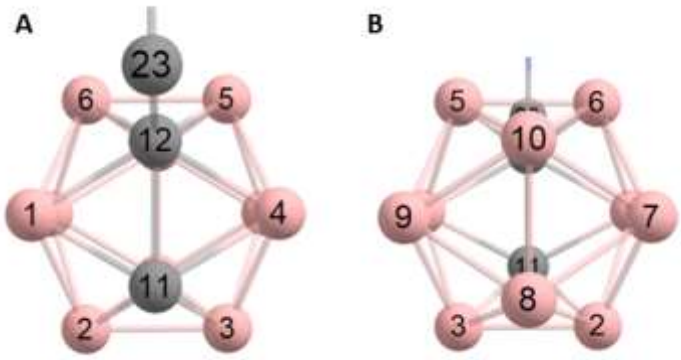

Figure S54. Top (**A**) and bottom (**B**) view of a structure model of **3**, geometry optimized at the B3LYP/Def2TZVP level of theory. The positions are numbered for NMR signal assignment and discussion of EFG tensors. The atoms of the side chain attached to carbon no. 23 is not shown here for clarity reasons. Hydrogen atoms are omitted for clarity.

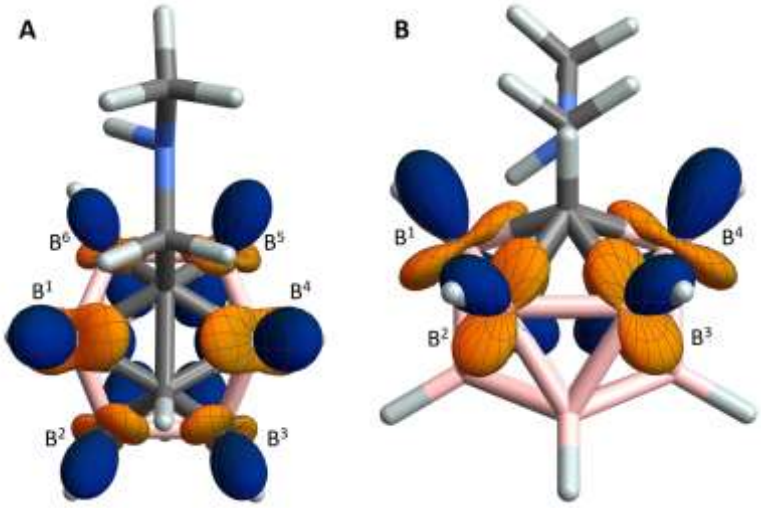

Figure S55. Top (**A**) and side (**B**) view onto a structure model of **3** with the EFG tensors shown at the boron positions 1-6. Colour coding and sign convention is analogous to **Figure S49**.

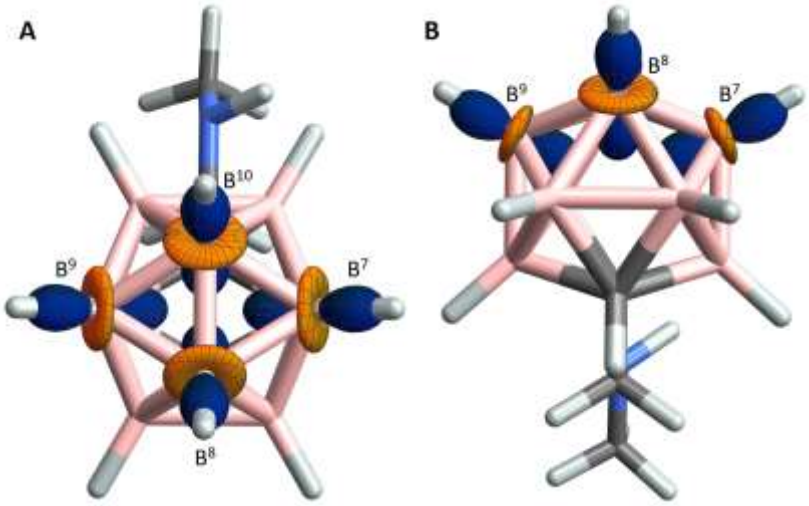

Figure S56. Top (**A**) and side (**B**) view onto a structure model of **3** with the EFG tensors shown at the boron positions 7-10. Colour coding and sign convention is analogous to **Figure S49**.

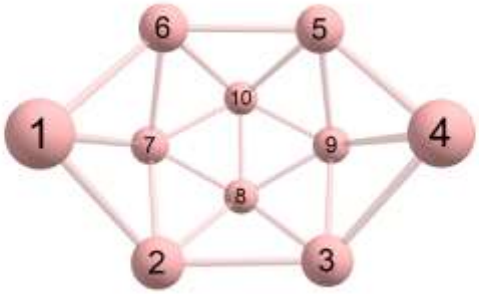

Figure S57. Structure model of **4**, geometry optimized at the B3LYP/Def2TZVP level of theory. The positions are numbered for NMR signal assignment and discussion of EFG tensors. Hydrogen atoms are omitted for clarity.

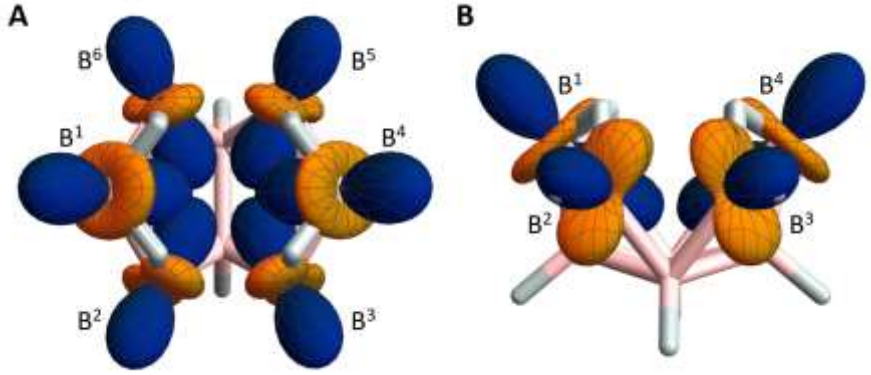

Figure S58. Top (**A**) and side (**B**) view onto a structure model of **4** with the EFG tensors shown at the boron positions 1-6. Colour coding and sign convention is analogous to **Figure S49**.

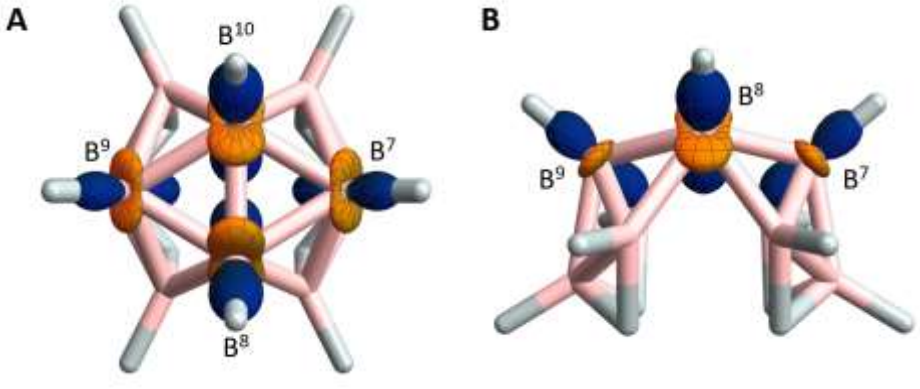

Figure S59. Top (**A**) and side (**B**) view onto a structure model of **4** with the EFG tensors shown at the boron positions 7-10. Colour coding and sign convention is analogous to **Figure S49**.

Experimentally determined and calculated tensors

Table S2. Alignment tensors determined from experimentally measured ^{11}B-^{1}H and ^{13}C-^{1}H RDCs.

	A_{xx}	A_{yy}	A_{zz}
1	-1.134E-04	-6.257E-04	7.391E-04
2	-1.598E-05	-5.413E-04	5.573E-04
3	-1.010E-04	-1.236E-04	2.246E-04
4	-2.876E-04	-4.112E-04	6.989E-04

Table S3. Alignment tensors determined from experimentally measured ^{11}B RQCs.

	A_{xx}	A_{yy}	A_{zz}
1	-2.358E-04	-5.746E-04	8.104E-04
2	4.783E-06	5.469E-04	-5.517E-04
3	-8.006E-05	-1.025E-04	1.925E-04
4	-2.548E-04	-3.521E-04	6.068E-04

All alignment tensors are given in the respective principal axis system of each compound following the convention $|A_{zz}|>|A_{yy}|>|A_{xx}|$ (see **Figure S44** - **Figure S47**).

Table S4. EFG tensors (eigenvalues, in atomic units) for the respective equivalent boron sites calculated for a geometry optimized model structure of **1** in the gas phase. The values are given according to the convention $|V_{zz}|>|V_{yy}|>|V_{xx}|$ using the Gaussian sign convention which is opposite to the more commonly used sign convention used by Autschbach *et. al.*[5] The numbering of the boron positions is shown in **Figure S48**.

	V_{xx} (a.u.)	V_{yy} (a.u.)	V_{zz} (a.u.)
1,4	-0.0759	-0.1443	0.2202
2,3,5,6	-0.0435	-0.1404	0.1839
7,9	-0.0673	-0.0816	0.1488
8,10	-0.0675	-0.0828	0.1502

Table S5. EFG tensors (eigenvalues, in atomic units) for the respective equivalent boron sites calculated for a geometry optimized model structure of **2** in the gas phase. The values are given according to the convention $|V_{zz}|>|V_{yy}|>|V_{xx}|$ using the Gaussian sign convention. The numbering of the boron positions is shown in **Figure S51**.

	V_{xx} (a.u.)	V_{yy} (a.u.)	V_{zz} (a.u.)
1,4	-0.0427	-0.1325	0.1752
2,3,5,6	-0.0338	-0.1406	0.1744
7,9	-0.0426	-0.1365	0.1791
8,10	-0.0663	-0.0805	0.1468

Table S6. EFG tensors (eigenvalues, in atomic units) for the respective equivalent boron sites calculated for a geometry optimized model structure of **3** in the gas phase. The values are given according to the convention $|V_{zz}|>|V_{yy}|>|V_{xx}|$ using the Gaussian sign convention. The numbering of the boron positions is shown in **Figure S54**.

	V_{xx} (a.u.)	V_{yy} (a.u.)	V_{zz} (a.u.)
1,4	-0.0706	-0.1469	0.2175
2,3	-0.0390	-0.1437	0.1827
5,6	-0.0422	-0.1392	0.1814
7,9	-0.0633	-0.0823	0.1456
8	-0.0689	-0.0784	0.1473
10	-0.0695	-0.0797	0.1492

Table S7. EFG tensors (eigenvalues, in atomic units) for the respective equivalent boron sites calculated for a geometry optimized model structure of **4** in the gas phase. The values are given according to the convention $|V_{zz}|>|V_{yy}|>|V_{xx}|$ using the Gaussian sign convention. The numbering of the boron positions is shown in **Figure S57**.

	V_{xx} (a.u.)	V_{yy} (a.u.)	V_{zz} (a.u.)
1,4	-0.1099	-0.1337	0.2425
2,3,5,6	-0.0532	-0.1618	0.2150
7,9	-0.046	-0.0824	0.1260
8,10	-0.0492	-0.1039	0.1532

1 a.u. = 9.717E-21 V/m^2

Q Factor Plots

In all cases, the Q factor was determined as introduced by Cornilescu *et. al.* according to Equation 1 (x = RDC, RQC):[6]

$$Q = \sqrt{\frac{\sum(x_{exp} - x_{calc})^2}{\sum x_{exp}}} \quad (1)$$

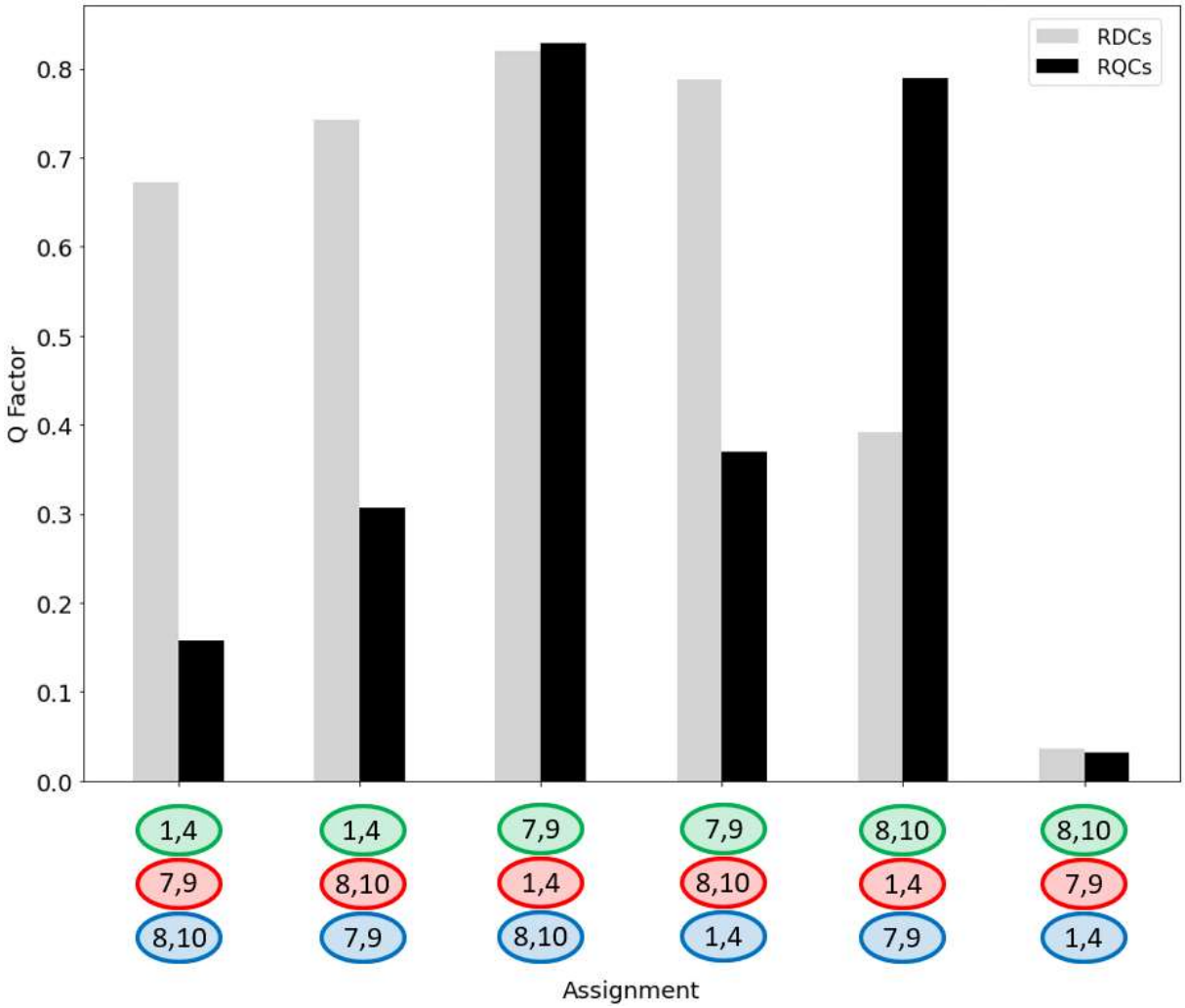

Figure S60. Q factors for all possible ^{11}B resonance assignments of **1** using either ^{11}B-^{1}H and ^{13}C-^{1}H RDCs (light gray) or ^{11}B RQCs (black). Colouring of the resonances is shown in **Figure 1B** in the main text.

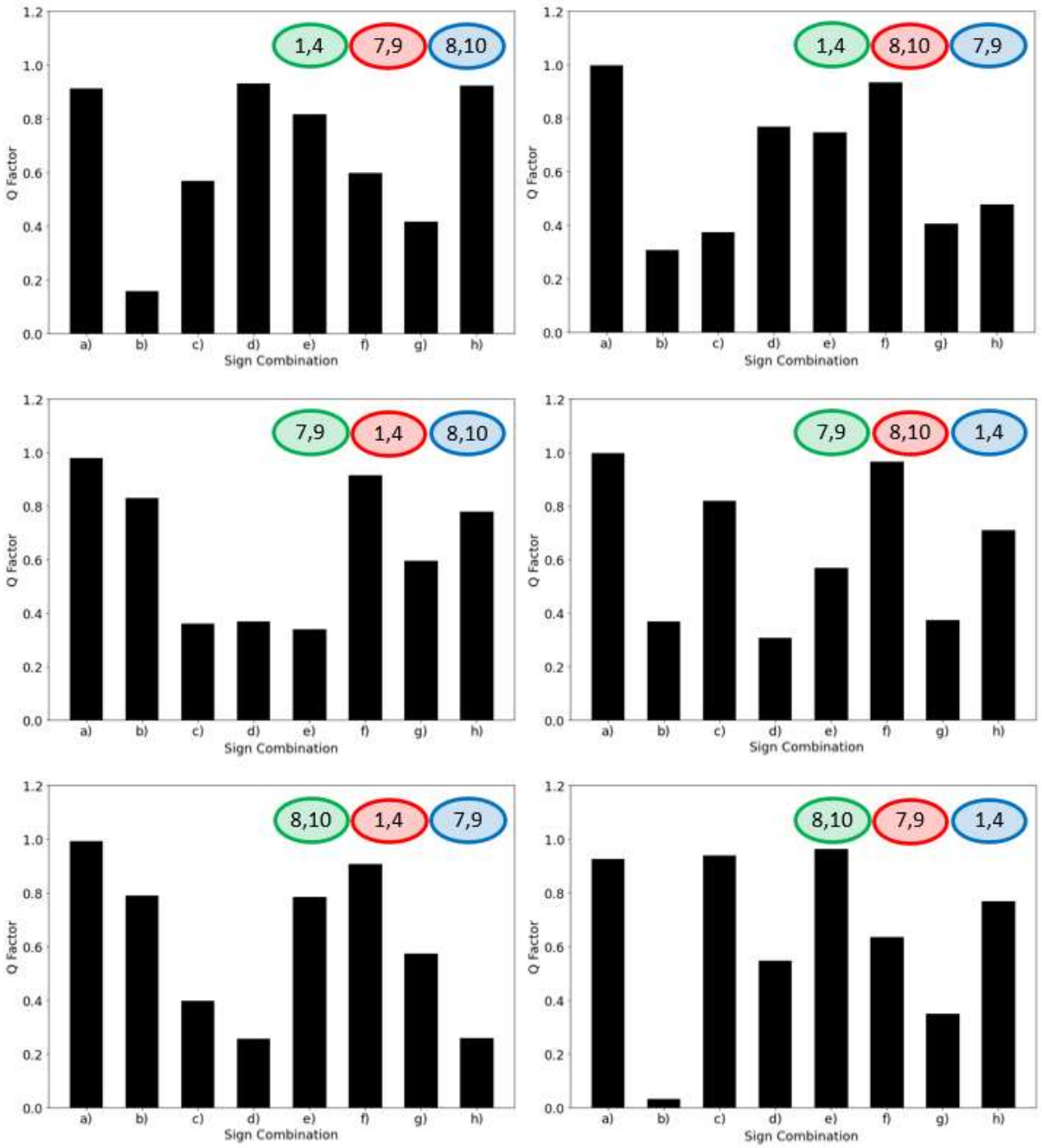

Figure S61. Q factors for all possible ^{11}B resonance assignments of **1** using ^{11}B RQCs with unknown sign. The six subfigures correspond to the six assignments as shown in **Figure S60** while the horizontal axis in each subfigure corresponds to the different sign combinations: a) all RQCs have the same sign, b) green + blue and red + yellow have the same sign, respectively, c) green + red and yellow + blue have the same sign, respectively, d) green + yellow and red + blue have the same sign, respectively, e) red + yellow + blue have the same sign, f) green + yellow + blue have the same sing, g) green + red + blue have the same sign and h) green + red + yellow have the same sign. Colouring of the resonances is as in **Figure 1B** in the main text and **Figure S10**.

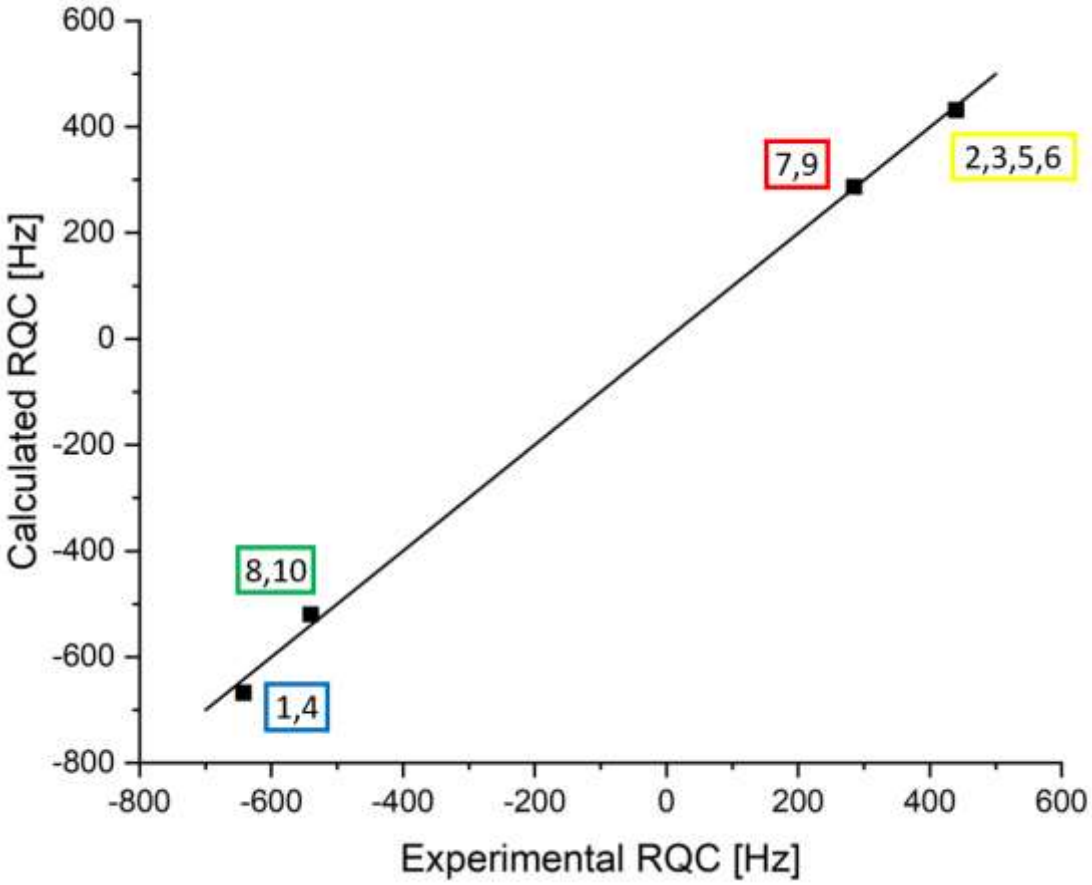

Figure S62. Experimental vs. calculated RQC values for the assignment possibility with the lowest Q factor (0.032) for **1**.

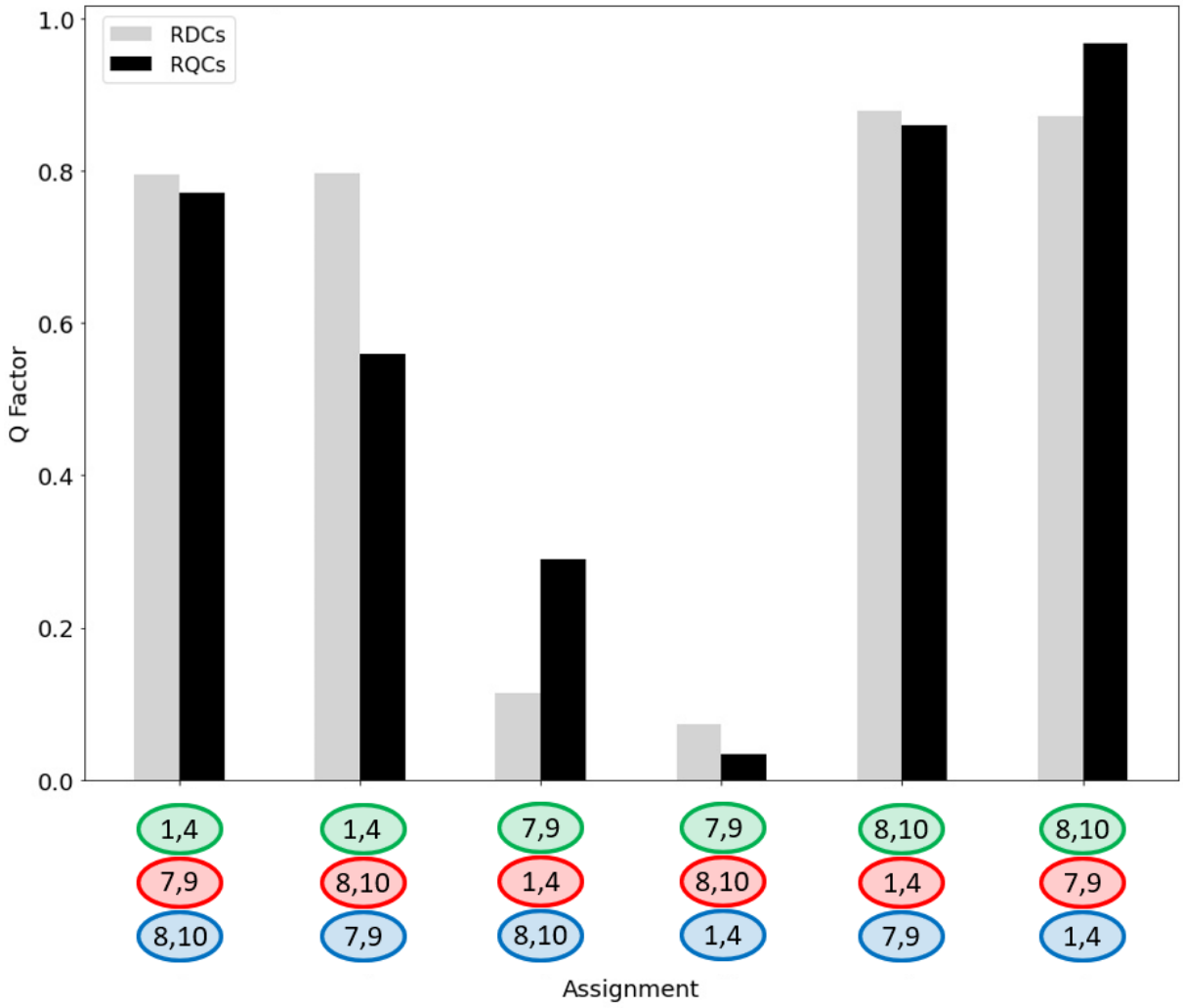

Figure S63. Q factors for all possible ^{11}B resonance assignments of **2** using either ^{11}B-^{1}H and ^{13}C-^{1}H RDCs (light gray) or ^{11}B RQCs (black). Colouring of the resonances is shown in **Figure S20**.

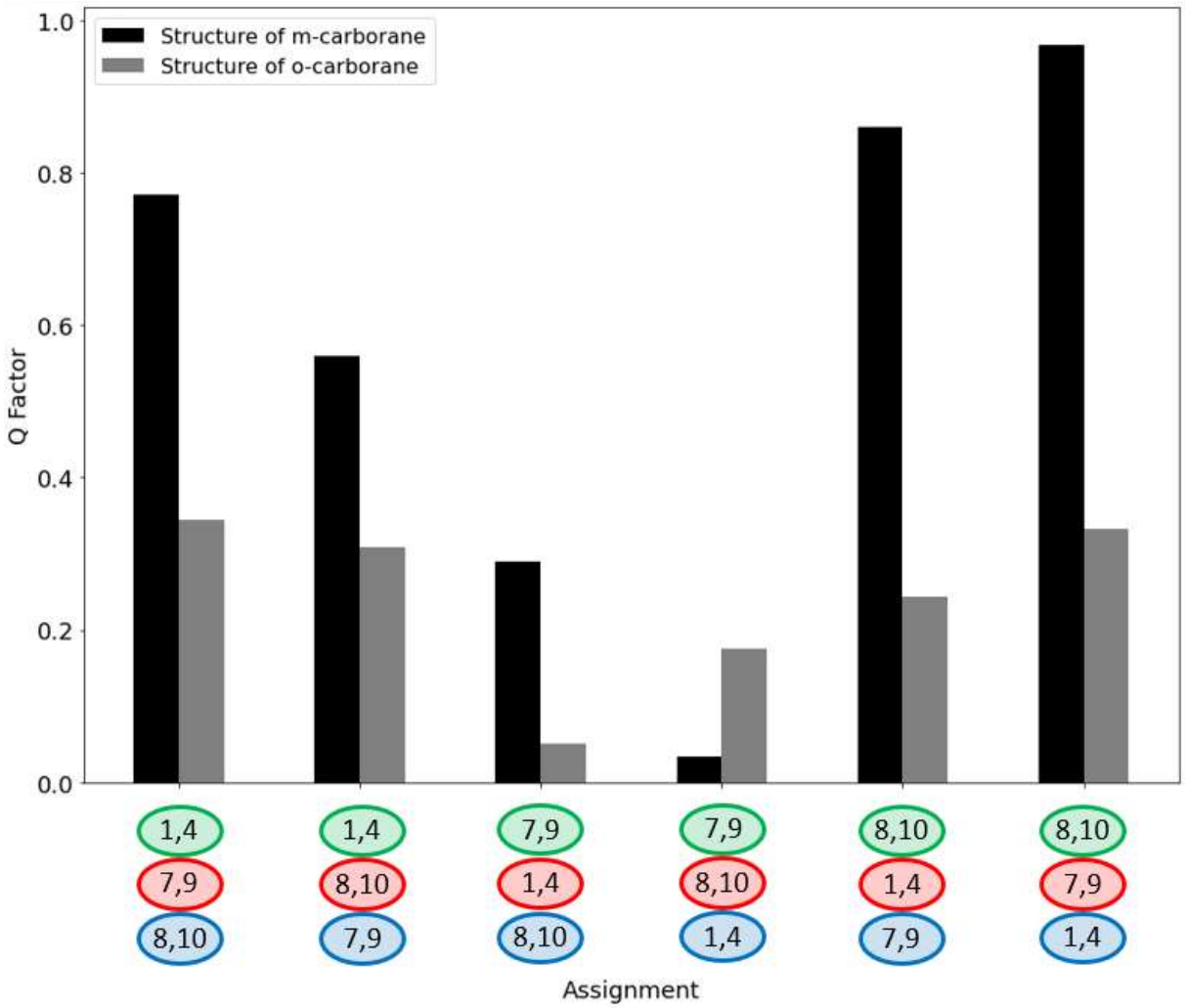

Figure S64. Q factors for all possible ^{11}B resonance assignments of **2** using ^{11}B RQCs on a structure model of **2** (black) and **1** (dark gray). Colouring of the resonances is shown in **Figure S20**.

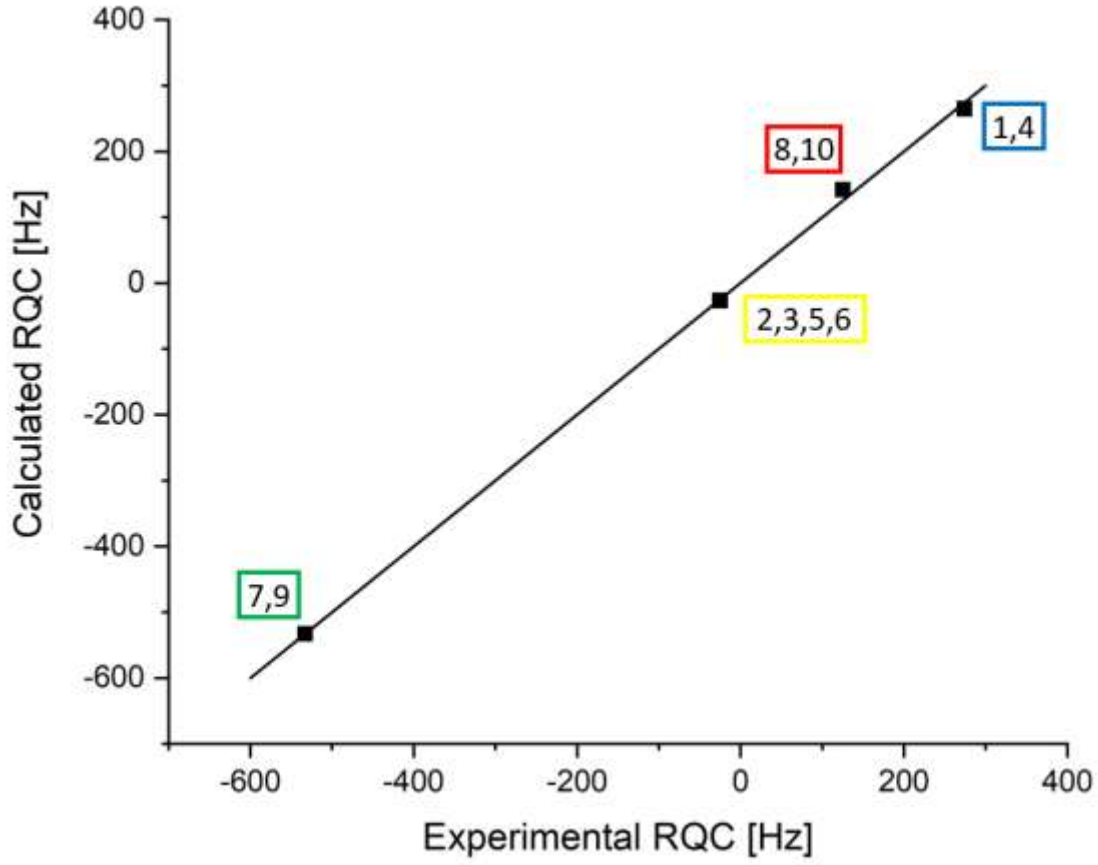

Figure S65. Experimental vs. calculated RQC values for the assignment possibility with the lowest Q factor (0.031) for **2**.

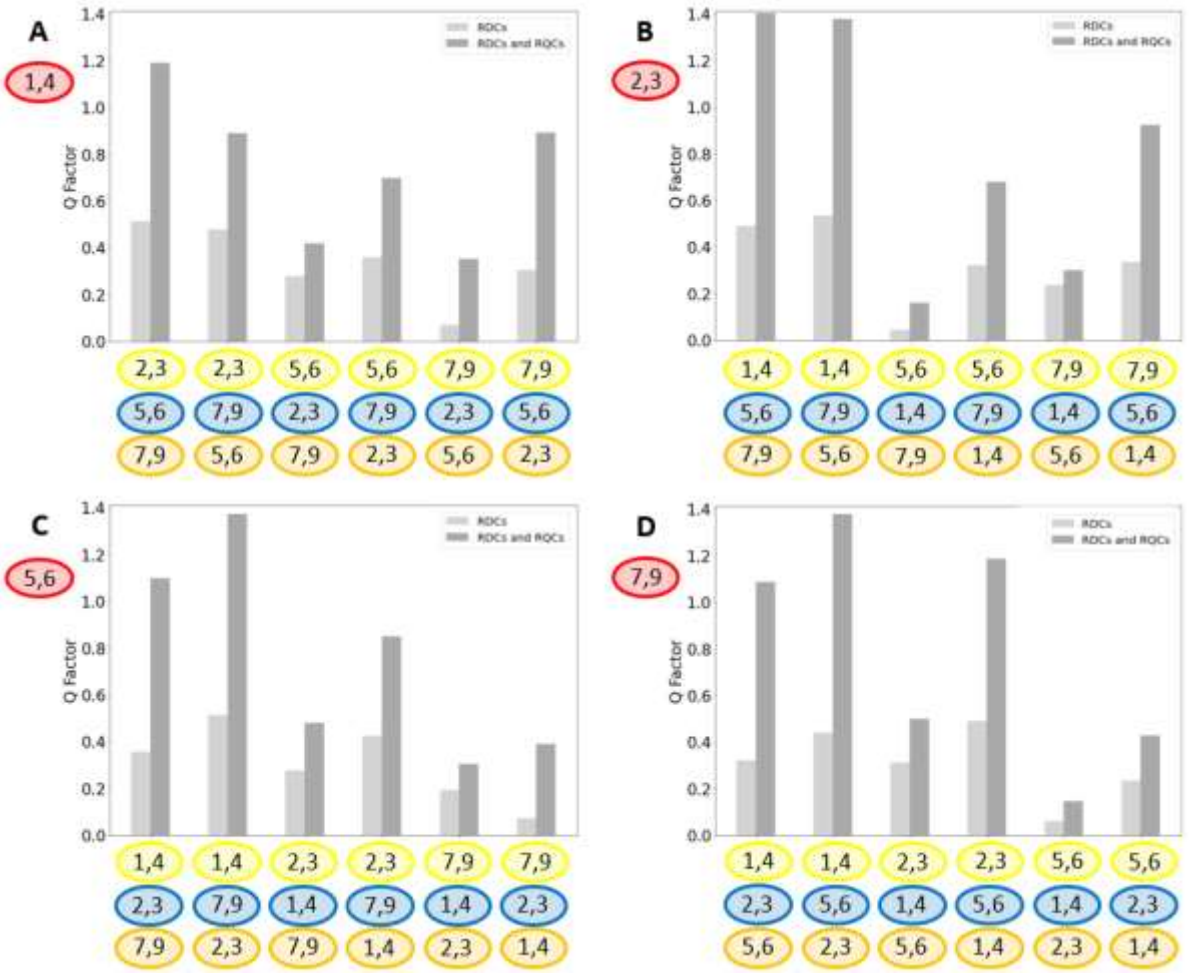

Figure S66. Q factors for all possible assignments of the four ^{11}B resonances between –9.42 and –13.38 ppm of **3** using ^{11}B-^{1}H and ^{13}C-^{1}H RDCs (light gray) and a combination of ^{11}B-^{1}H, ^{13}C-^{1}H RDCs and ^{11}B RQCs (dark gray). For each subfigure **A**, **B**, **C** and **D**, the resonance marked in red at –9.42 ppm was fixed to one of the positions B^1/B^4, B^2/B^3, B^5/B^6 and B^7/B^9, respectively. In all cases, the two resonances marked in light and dark green at –3.29 and –5.72 ppm are already assigned to the positions B^{10} and B^8, respectively. Colouring of the resonances is shown in **Figure S30**.

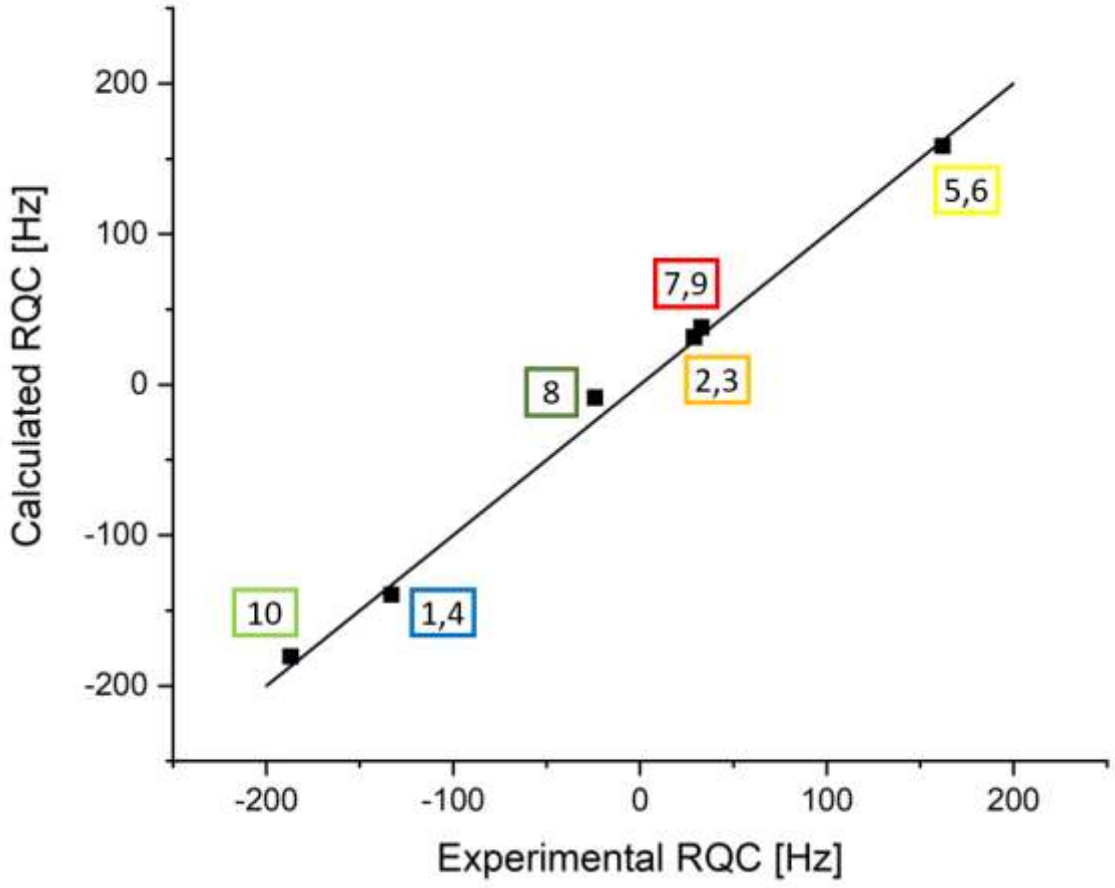

Figure S67. Experimental vs. calculated RQC values for the assignment possibility with the lowest Q factor (0.063) for **3**.

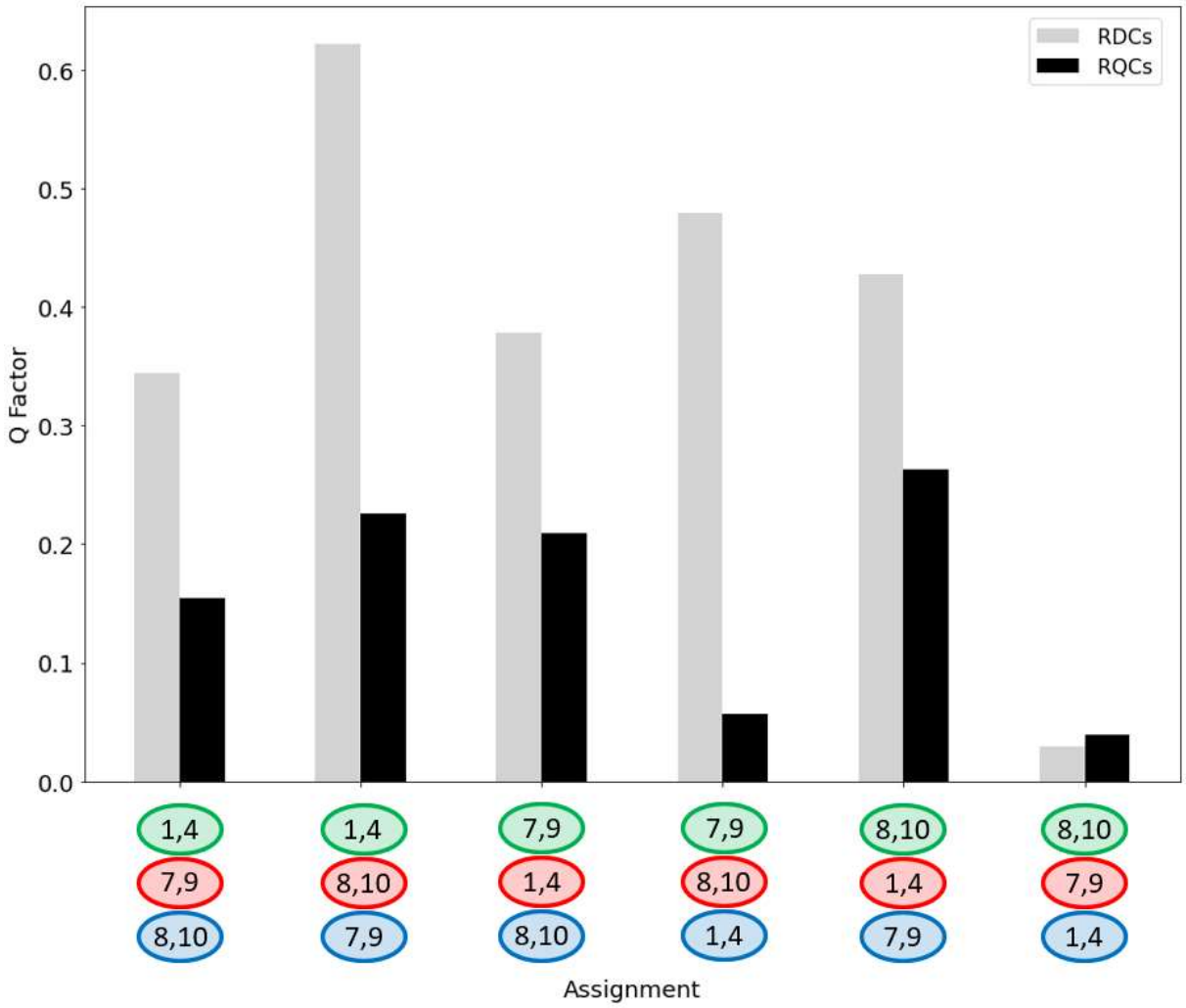

Figure S68. Q factors for all possible ^{11}B resonance assignments of **4** using either ^{11}B-^{1}H RDCs (light gray) or ^{11}B RQCs (black). Colouring of the resonances is shown in **Figure S40**.

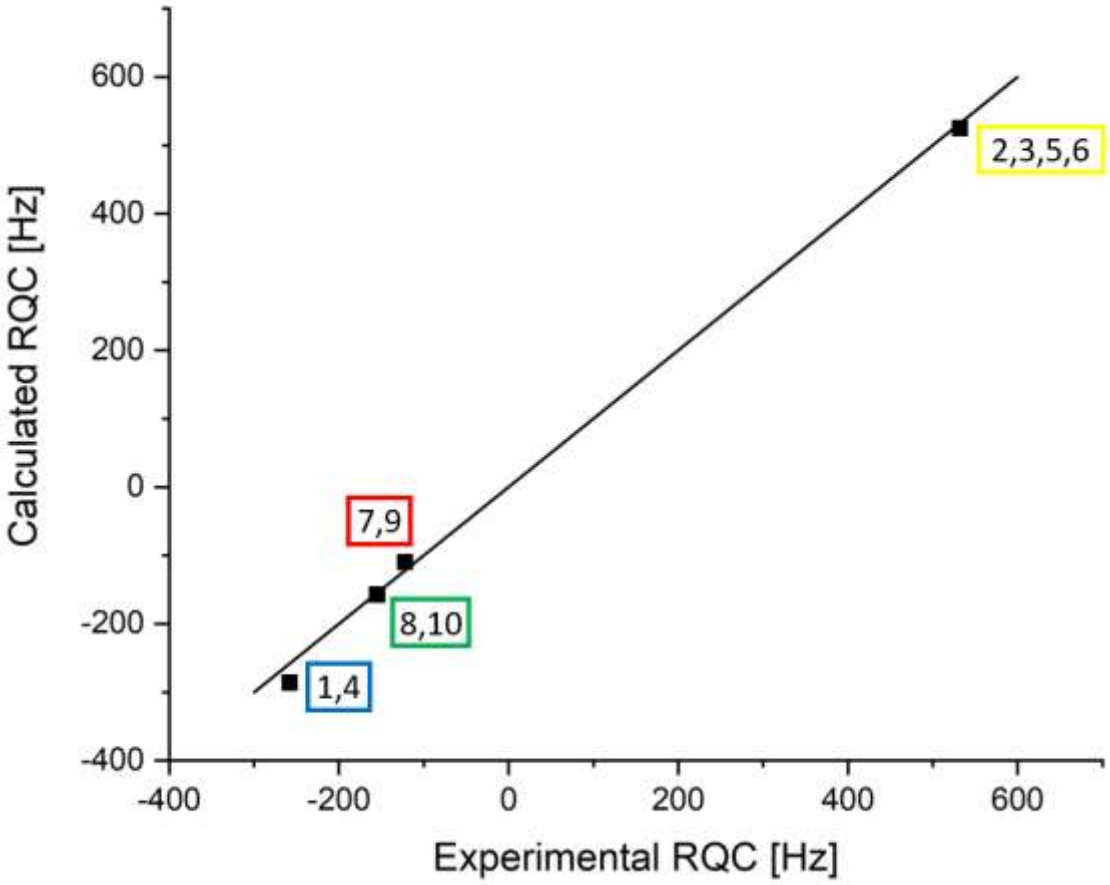

Figure S69. Experimental vs. calculated RQC values for the assignment possibility with the lowest Q factor (0.039) for **4**.

References

[1] A. Navarro-Vázquez, *Magn. Reson. Chem.* 2012, **50**, S73-S79.

[2] M. J. Frisch, G. W. Trucks, H. B. Schlegel, G. E. Scuseria, M. A. Robb, J. R. Cheeseman, G. Scalmani, V. Barone, G. A. Petersson, H. Nakatsuji, X. Li, M. Caricato, A. V. Marenich, J. Bloino, B. G. Janesko, R. Gomperts, B. Mennucci, H. P. Hratchian, J. V. Ortiz, A. F. Izmaylov, J. L. Sonnenberg, D. Williams-Young, F. Ding, F. Lipparini, F. Egidi, J. Goings, B. Peng, A. Petrone, T. Henderson, D. Ranasinghe, V. G. Zakrzewski, J. Gao, N. Rega, G. Zheng, W. Liang, M. Hada, M. Ehara, K. Toyota, R. Fukuda, J. Hasegawa, M. Ishida, T. Nakajima, Y. Honda, O. Kitao, H. Nakai, T. Vreven, K. Throssell, J. A. Montgomery, Jr., J. E. Peralta, F. Ogliaro, M. J. Bearpark, J. J. Heyd, E. N. Brothers, K. N. Kudin, V. N. Staroverov, T. A. Keith, R. Kobayashi, J. Normand, K. Raghavachari, A. P. Rendell, J. C. Burant, S. S. Iyengar, J. Tomasi, M. Cossi, J. M. Millam, M. Klene, C. Adamo, R. Cammi, J. W. Ochterski, R. L. Martin, K. Morokuma, O. Farkas, J. B. Foresman, and D. J. Fox, *Gaussian16*, Gaussian, Inc., Wallingford CT, 2016.

[3] a) F. Weigend, R. Ahlrichs, *Phys. Chem. Chem. Phys.* **2005**, *7*, 3297; b) F. Weigend, *Phys. Chem. Chem. Phys.* 2006, **8**, 1057.

[4] E. Zurek, C. J. Pickard, J. Autschbach, *J. Phys. Chem.* 2008, **C112**, 11744.

[5] J. Autschbach, S. Zheng, R. W. Schurko, *Concepts Magn. Reson.* 2010, **36A**, 84.

[6] G. Cornilescu, J. L. Marquardt, M. Ottiger, A. Bax, *J. Am. Chem. Soc.* **1998**, *120*, 6836.